The choice of baseline period influences the assessments of the outcomes of Stratospheric Aerosol Injection

Daniele Visioni[1], Douglas G MacMartin[2], Ben Kravitz[3], Ewa M. Bednarz[4], and Paul Brent Goddard[5]

[1]Department of Earth and Atmospheric Sciences
[2]Cornell University
[3]Indiana University
[4]CIRES / NOAA CSL
[5]Indiana University Bloomington

June 1, 2023

Abstract

The specifics of the simulated injection choices in the case of Stratospheric Aerosol Injections (SAI) are part of the crucial context necessary for meaningfully discussing the impacts that a deployment of SAI would have on the planet. One of the main choices is the desired amount of cooling that the injections are aiming to achieve. Previous SAI simulations have usually either simulated a fixed amount of injection, resulting in a fixed amount of warming being offset, or have specified one target temperature, so that the amount of cooling is only dependent on the underlying trajectory of greenhouse gases.

Here, we use three sets of SAI simulations achieving different amounts of global mean surface cooling while following a middle-of-the-road greenhouse gas emission trajectory: one SAI scenario maintains temperatures at 1.5ºC above preindustrial levels (PI), and two other scenarios which achieve additional cooling to 1.0ºC and 0.5ºC above PI.

We demonstrate that various surface impacts scale proportionally with respect to the amount of cooling, such as global mean precipitation changes, changes to the Atlantic Meridional Overturning Circulation (AMOC) and to the Walker Cell. We also highlight the importance of the choice of the baseline period when comparing the SAI responses to one another and to the greenhouse gas emission pathway.

This analysis leads to policy-relevant discussions around the concept of a reference period altogether, and to what constitutes a relevant, or significant, change produced by SAI.

The choice of baseline period influences the assessments of the outcomes of Stratospheric Aerosol Injection

D. Visioni[1,2], E. M. Bednarz[3,4,5], D. G. MacMartin[5], B. Kravitz[6,7] and P. B. Goddard[6]

[1]Department of Earth and Atmospheric Sciences, Cornell University, Ithaca, NY, USA
[2]Atmospheric Chemistry Observations & Modeling, National Center for Atmospheric Research, Boulder, CO, USA
[3]Cooperative Institute for Research in Environmental Sciences (CIRES), University of Colorado Boulder, Boulder, CO, USA
[4]NOAA Chemical Sciences Laboratory (NOAA CSL), Boulder, CO, USA
[5]Sibley School of Mechanical and Aerospace Engineering, Cornell University, Ithaca, NY, USA
[6]Department of Earth and Atmospheric Sciences, Indiana University, Bloomington, IN, USA
[7]Atmospheric Sciences and Global Change Division, Pacific Northwest National Laboratory, Richland, WA, USA

Key Points:

- We analyze results from a set of simulations considering various amounts of cooling using stratospheric aerosols.
- Many of the climatic responses at the surface can be considered linearly related to the amount of cooling.
- The choice of the specific baseline period influences these conclusions.

Corresponding author: Daniele Visioni, `dv224@cornell.edu`

Abstract

The specifics of the simulated injection choices in the case of Stratospheric Aerosol Injections (SAI) are part of the crucial context necessary for meaningfully discussing the impacts that a deployment of SAI would have on the planet. One of the main choices is the desired amount of cooling that the injections are aiming to achieve. Previous SAI simulations have usually either simulated a fixed amount of injection, resulting in a fixed amount of warming being offset, or have specified one target temperature, so that the amount of cooling is only dependent on the underlying trajectory of greenhouse gases.

Here, we use three sets of SAI simulations achieving different amounts of global mean surface cooling while following a middle-of-the-road greenhouse gas emission trajectory: one SAI scenario maintains temperatures at 1.5ºC above preindustrial levels (PI), and two other scenarios which achieve additional cooling to 1.0ºC and 0.5ºC above PI.

We demonstrate that various surface impacts scale proportionally with respect to the amount of cooling, such as global mean precipitation changes, changes to the Atlantic Meridional Overturning Circulation (AMOC) and to the Walker Cell. We also highlight the importance of the choice of the baseline period when comparing the SAI responses to one another and to the greenhouse gas emission pathway.

This analysis leads to policy-relevant discussions around the concept of a reference period altogether, and to what constitutes a relevant, or significant, change produced by SAI.

Plain Language Summary

By adding CO_2 to the atmosphere, the planet warms. As the primary energy input to the system is the Sun, you can try to balance this warming by slightly reducing the incoming sunlight, for example by adding tiny reflecting particles to the atmosphere (aerosols). This cooling will not perfectly cancel the warming from CO_2 due to different physical mechanisms. Understanding how the resulting climate from both effects changes requires a comparison with a "base" state: but there isn't one single choice, something which is made even more clear once one considers multiple amounts of cooling one could do. There isn't only one option as one could decide to just prevent future warming (or some of it), or also try to cancel warming that already happened. Here we explore how the projected outcomes can depend on the base state one selects and which change are linear with the amount of cooling achieved.

1 Introduction

The adverse global impacts produced by human-induced surface warming are well-documented in over 30 years of previous scientific literature and international proceedings. In 1990, the first Intergovernmental Panel on Climate Change (IPCC) Assessment Report already highlighted many of the future challenges and laid the ground for the creation of the United Nations Framework Convention on Climate Change (UNFCCC). The second Assessment Report, in 1995, was essential in informing policy makers on their way to approve the Kyoto Protocols in 1997, where the first legally binding commitment to reduce emissions (by 5% compared to 1990 levels) was ratified. By the time of the Fourth and Fifth assessment reports, observations of rising greenhouse gas (GHG) emissions and concentrations and increasing surface temperatures led the scientific community and the parties of the UNFCCC to determine new emission commitments. These commitments were not just based on emission targets, but also on global mean temperature "thresholds" that the world should commit to not trespassing during this century in order to avoid the worst effects of climate change (Gao et al., 2017). The Paris Agreement clearly stated that the parties were bound (Rajamani & Werksman, 2018) to limit global warming to well below 2, and pursue efforts to limit temperature increase to 1.5 $^{\mathrm{o}}$C, compared to pre-industrial levels. The need for such thresholds was highlighted in the IPCC Special Report on Global Warming of 1.5°C (Masson-Delmotte et al., 2018), where the risks of staying below 1.5$^{\mathrm{o}}$C as compared to 2$^{\mathrm{o}}$C was discussed in depth.

More recently, multiple studies have shown how countries' commitments and actions are faring against these temperature targets determined in the Paris Agreement, with the general agreement being that almost none of the signatories are actually close to achieving the emission cuts necessary in the short term to remain below 1.5$^{\mathrm{o}}$C (e.g., Kriegler et al. (2018); Brecha et al. (2022)). The current IPCC emission scenarios that maintain temperatures below this threshold (with or without a temporary overshoot) make use of large assumptions of the scalability and deployability of carbon dioxide removal (CDR) technologies in the future (Haszeldine et al., 2018), which some have criticized as unrealistic (Holz et al., 2018; Boettcher et al., 2021; Warszawski et al., 2021). This non-exhaustive and brief description of the last decades of climate change serves here to highlight a conundrum: the risks of surface temperatures going above 1.5$^{\mathrm{o}}$C above preindustrial get clearer with every passing year, and that temperature threshold risks being reached in the next two decades, yet, actual emission cut pledges by all nations that would serve to curtail that warming are not matching what is in international agreement, and the need for a rapid ramping up of CDR necessary to avoid an overshoot (Kriegler et al., 2018) is not matched by current developments in that area.

A potential additional element of a policy response in the short term, allowing for temperatures (and risks) to be managed while emissions are reduced was already discussed by (Crutzen, 2006) with the proposal to reduce a portion of the incoming sunlight by means of injecting sulfate aerosol precursors into the lower stratosphere (Stratospheric Aerosol Injections, SAI hereafter), in order to produce an optically active cloud of aerosol particles with a long lifetime. Crutzen already highlighted risks as well: not only those in the physical realm (changes in stratospheric composition, differences in the forcing of GHG and of the produced aerosols resulting in a climate different from that produced by a reduction of GHG concentrations) but also those in the human and policy realm, namely that the idea itself of SAI could interfere with emission abatements because of the perception that an "easier" option is available. Research in the last two decades has tried to better understand both of those kinds of risks. In the physical sphere, this has been done mainly by simulating the potential effects of simplified SAI deployment scenarios in global climate models, either by injecting some quantity of SO_2 or of other aerosols in the tropical lower stratosphere (Robock et al., 2008; Kravitz et al., 2015), or by simply reducing the solar constant at the top of the model as a proxy (Niemeier et al., 2013; P. Irvine et al., 2019; Visioni, MacMartin, Kravitz, Boucher, et al., 2021; Visioni, MacMartin, & Kravitz, 2021).

In order to understand the impacts of global warming – which ultimately depend on how much greenhouse gas is emitted – the IPCC usually evaluates multiple future scenarios. As the effects of SAI similarly depend on how it is done (e.g., Kravitz et al. (2019)), one cannot make conclusions about the impacts of SAI by only analyzing one scenario. In terms of the magnitude of cooling to achieve, different areas of the world might desire different amounts, and that simply slowing down the warming (MacMartin et al., 2018; P. Irvine et al., 2019), or keeping it at the Paris Agreement threshold of 1.5$^{\mathrm{o}}$C above preindustrial might not be enough for them to stave off the worst or most long term impacts from climate change such as sea level rise (P. J. Irvine et al., 2012). Trade offs between larger coolings and larger impacts from stronger interventions need to be better determined: in (MacMartin et al., 2022) we explained the rationale behind our new sets of simulations which will be used in this work, in which we compare a scenario where, under SSP2-4.5 emissions, SAI is used to keep temperatures at 1.5$^{\mathrm{o}}$C above preindustrial with two other scenarios that further cool by 0.5$^{\mathrm{o}}$C and 1.0$^{\mathrm{o}}$C below that level.

Here we further explore our set of scenarios, leveraging the combination of different comparison periods and of scenarios with different cooling amounts to discuss both the linearity of the surface climate response and to highlight how important the choice of a reference period is when discussing the potential outcomes of SAI. In the following section we will briefly describe the climate model used for this study and then explain more in depth the functioning of the feedback algorithm that determines how to inject SO_2 to achieve the temperature targets in the three SAI scenarios (Section 2). We will then discuss the outcomes in terms of sulfate burden (Section 3.1), surface temperature (Section 3.2) with a focus on the tropical Eastern Pacific response (Section 3.2.1), Atlantic Meridional Overturning Circulation (Section 3.3) and global and regional precipitation (Section 3.4; these all provide examples where the choice of reference period influences interpretations.

2 Methods

2.1 Climate model

In this study we use the Community Earth System Model Version 2 (CESM, Danabasoglu et al. (2020)) in its Whole Atmosphere Community Climate Model Version 6 (WACCM6) configuration with simplified tropospheric chemistry (Davis et al., 2022), hereafter CESM2-WACCM6. This model version has a horizontal resolution of 1.25º longitude by 0.9º latitude with 70 vertical levels that extend up to about 140km. The version we use has comprehensive stratospheric and upper-atmospheric chemistry, as well as an interactive aerosol microphysics scheme termed the Modal Aerosol Module (MAM4) (Liu et al., 2016), but has simplified tropospheric chemistry that only includes the most relevant processes and does not have detailed Secondary Organic Aerosol (SOA) chemistry; in (Davis et al., 2022), this has been shown to not produce relevant changes in stratospheric chemistry and surface climate.

2.2 Simulations design

We consider here three SAI scenarios spanning the period 2035 to 2070, each of which injects the appropriate (more details provided shortly) SO_2 magnitudes required to keep global mean surface temperatures at 1.5ºC, 1.0ºC or 0.5ºC above the preindustrial levels (PI, with the 2020-2039 mean of the CESM model surface temperature data defined as corresponding to the 1.5ºC above PI), respectively (henceforth referred to as SAI-1.5, SAI-1.0, SAI-0.5); motivation and description is given in MacMartin et al 2022. In all cases, GHG emissions follow the Shared Socioeconomic Pathway (SSP) 2-4.5 (Meinshausen et al., 2020).

The SO_2 is injected at every time step, every day of the year at 4 off-equatorial locations - 30ºN, 15ºN, 15ºS and 30ºS, and the yearly injection rates are determined independently at the beginning of each year using a feedback algorithm as in Kravitz et al. (2017). The algorithm computes the injection rates by comparing the annual mean near-surface air temperatures simulated over the previous year to determine how much those values differ from the desired target. This is done not just for global mean near-surface temperature (T0) but also the difference in temperatures between the two hemispheres, computed using the projection of the zonal mean surface temperature onto the first Legendre polynomial (eq. here), and the difference in temperatures between the poles and the equator, computed using the projection onto the second Legendre polynomial ($\ell_0 = 1$, $\ell_1 = \sin(\psi)$, and $\ell_2 = 3(\sin^2(\psi) - 1)/2$, where ψ is the latitude). The target values can be tied to periods in the baseline simulations when T0 had the same 20-year average value: so for SAI-1.5, the period over which T0 is 1.5ºC above PI is 2020-2039 (by definition of our simulations). For SAI-1.0 and SAI-0.5, these periods are 2008-2027 and 1993-2012, respectively, which corresponds to T0 values that are 0.5ºC and 1.0º lower than for the SAI-1.5. Determining this time-period of reference is necessary to calculate the target values for T1 and T2: for all scenarios, these two targets are the values averaged over the reference period.

The controller algorithm uses these targets to determine the needed yearly injection rates of SO_2 at the four latitudes, by estimating the needed projections of the zonal mean stratospheric aerosol optical depth (sAOD) onto the same Legendre polynomials to achieve them and then estimating the injections rates necessary to achieve those sAOD patterns. Information on how the injection of a certain amount of SO_2 translated to a certain shape of sAOD and to a certain temperature response are derived from single-point sensitivity simulations that have been described in Visioni et al. (2023), where all information is available to reproduce the calculations with similar sensitivity simulations in other climate models. The presence of the feedback algorithm is not trying to represent how operationally SAI would work in the real world but should be viewed instead as a modeling tool to allow us to "learn" the set of injection rates needed to achieve a given set of targets.

In all cases, we analyze the responses over the last 20 years of the SAI simulations (i.e. 2050-2069), and compare them against each of the respective baseline periods with the same global mean surface temperature, as well as against the same quasi-present day period, here chosen as the mean over 2020-2039.

2.3 Simulated injection rates

In Figure 1 we show the connection between the imposed SO_2 injection rates and the resulting sAOD patterns and the magnitudes of the global mean cooling. In the top part, we show the total injection rates in the three sets of simulations. In the case of the SAI-1.5 simulation the target (1.5ºC above PI) is reached just a few years before the start of SAI in 2035; therefore the injection rate can be allowed to slowly build up to offset the corresponding global warming (Fig. 1a). In contrast, for SAI-1.0 and SAI-0.5 a "ramp-up" time of 10 years has been built in in the controller to gradually achieve the desired temperature target (and so to avoid a steep temperature change over a few years). After that, changes in injection rates are similar to SAI-1.5, i.e. to just offset the warming from GHGs in SSP2-4.5.

While global mean temperature changes can be tied to the overall injection rates, the management of the other two targets (T1 and T2) depend on the distribution of injection rates over the four locations. Figure 1b shows this distribution as a fraction of the overall injection rates (thereby accounting for the differences in total magnitudes). The distribution of the injection rate during the second part of the simulation (after the initial 10 years) depends on the ratio dT1/dT0 and dT2/dT0 (calculated as the value of T in the reference period minus that in the 2050-2069 period and shown in Table S1), which in turns affect the L1/L0 and L2/L0 ratio needed, which influences the amounts at the various injection locations (MacMartin et al., 2017). In all three cases over half of the injection is determined to be at 15ºS and 15ºN, and the remnant at 30ºS, with no injection at 30ºN. The distribution of injection rates at the onset of SAI is not necessarily consistent in the first 10 years, i.e before the controller converges, as the initial period is influenced by the convergence time of the algorithm and by the initial best guess (based on the sensitivity to the fixed injection rates shown in Visioni et al. (2023)). The hemispheric asymmetry in injection rates is discussed (for simulations in slightly different model configuration) in (Fasullo & Richter, 2023).

In panels 1c-e), we show the projections of the achieved sAOD patterns on the first three Legendre polynomials (termed L0, L1, L2), which relate to the overall magnitude of injection (panel 1a) for L0 and to the locations of the injections for L1 and L2, which indicate how much difference there is in sAOD between the hemispheres (L1) and between tropical and high latitudes (L2) (Ban-Weiss & Caldeira, 2010). In Fig. S1, we also show the relationship between the actual sAOD and the internal control variables indicating the expected values by the controller based on the response in the fixed injection. If the relationship between injection rates and L0, L1, L2 remained linear, then the expected L0, L1, L2 would match the actual. Fig. S1 shows that while the match is very good for SAI-1.5, for higher temperature targets the controller assumes that less SO_2 is

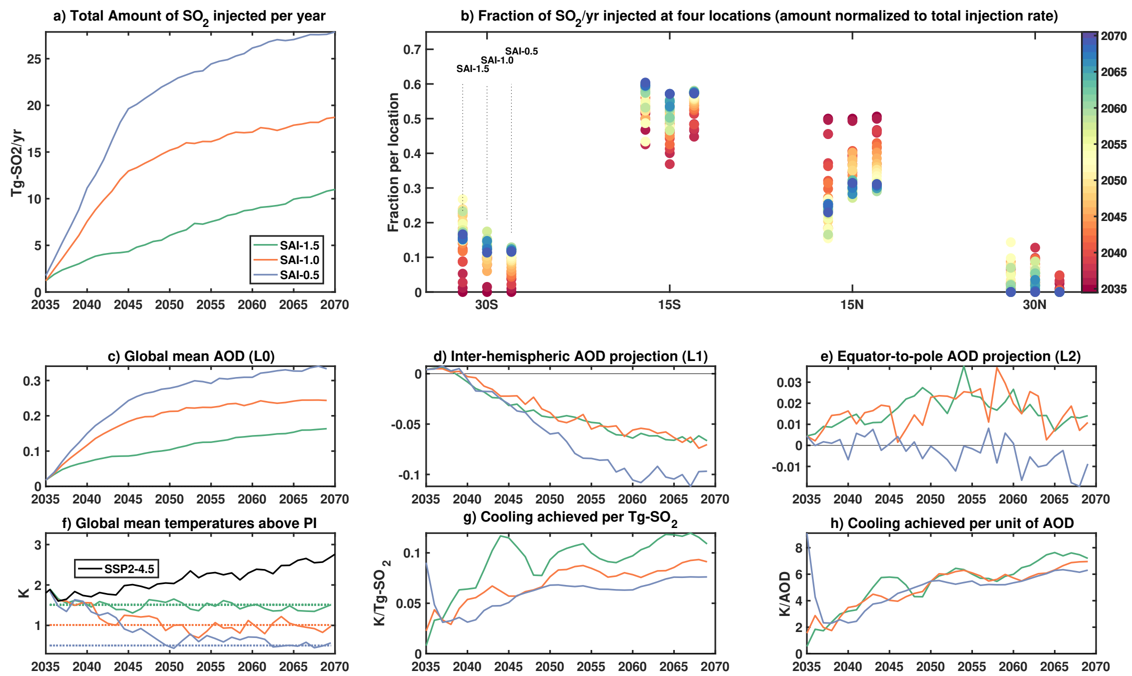

Figure 1. a) Total injection rates in the three sets of SAI simulations. b) Distribution of the injection rates at the four injection locations (30ºS, 15ºS, 15ºN, 30ºN), shown as the fraction of the total amount, color-coded depending on the year from red (2035) to blue (2070); SAI-1.5 is always the leftmost set, followed by SAI-1.0 and SAI-0.5. c-e) Values of L0 (global mean sAOD), L1 (inter-hemispheric sAOD projection) and L2 (equator-to-pole sAOD projection). f) Global cooling achieved in the SAI simulations compared to preindustrial (PI) temperatures. g) Efficacy of cooling per 1 Tg of SO_2 injected. h) Efficacy of cooling per sAOD produced. A 5-years running mean is applied to panels g) and h). For clarity, only the ensemble averages are shown in all panels.

needed to achieve a certain sAOD pattern. This points to nonlinearities in the injection rate to AOD conversion under high injection rates, which could arise from larger effective radii and shorter aerosol lifetime (particularly for L0) and from dynamical changes in the stratospheric transport (for L1 and L2) due to stronger lower stratospheric warming in the tropics (Visioni, MacMartin, Kravitz, Lee, et al., 2020). The differences in L1 for SAI-0.5 are driven by a value of dT1/dT0 (Table S1) that is 28% larger compared to that in SAI-1.5; similarly, the L2 differences are driven by a dT2/dT0 value that is 25% smaller in SAI-0.5 compared to SAI-1.5.

Figure 1f shows the simulated global mean temperatures above PI conditions and, thus, illustrates the overall cooling achieved in the three simulations compared to the warming in the SSP2-4.5 scenario (also shown in MacMartin et al. (2022)). Over the last 20 years of the three SAI simulations, the difference in global mean temperatures compared to the same period in SSP2-4.5 is 0.9 ºC (SAI-1.5), 1.4 ºC (SAI-1.0) and 1.8 ºC (SAI-0.5). Finally, in panels g) and h) we show how this cooling relates to the injected amount of SO_2 and to the unit of global mean AOD. We find that the relationship between the total SO_2 injection and the resulting global mean cooling is sublinear (i.e. the strongest efficacy is found for SAI-1.5); similarly, a lower cooling per unit AOD is achieved, with a value of 6.5, 6.1 and 5.7 K/AOD for SAI-1.5, SAI-1.0 and SAI-0.5 respectively. Both sublinearities are due to microphysical nonlinearities (Niemeier & Timmreck, 2015; Visioni, MacMartin, Kravitz, Lee, et al., 2020) as larger aerosols have lower lifetime as they're heavier and they are also less efficient scatterer (Laakso et al., 2022). Hence, while 10 Tg-SO_2 are necessary in SAI-1.5 to cool by 1ºC, the next 10 Tg-SO_2 only cool by 0.7ºC in SAI-0.5, thereby requiring 26 Tg-SO_2 to cool to the desired target of 1.8 ºC, instead of 18 Tg-SO_2 if the relationship had remained the same as in SAI-1.5.

3 Results

3.1 Sulfate burden

In Figure 2 we show the changes in the stratospheric sulfate burden produced by the injections described in Section 2.3. A comparison of panels a-c) highlights the large differences in the sulfate concentrations between the three SAI strategies, in line with the differences in cooling and injection rates reported in Fig. 1. SAI-1.5 increases the sulfate burden by up to 40 μg-S/kg-air in the tropical lower stratosphere (as compared to 1 μg-S/kg-air in the unperturbed stratosphere, while SAI-0.5 peaks at 108 μg-S/kg-air). Similarly, the overall increase in column burden as shown in panel 2d is 20.2 mg-S/m2 for SAI-1.5 and 52.6 mg-S/m2 for SAI-0.5. Despite large differences in total sulfate burden, all 3 SAI simulations show similar horizontal distributions with the largest sulfate burden (Fig. 2d) and sAOD (Fig. 2e) increases in the Southern Hemisphere, consistent with the similarities in the distributions of the injection rates in Fig. 1b. The significantly larger (by a factor of $\sim$2) amount of aerosols in the Southern Hemisphere than the Northern Hemisphere is necessary in this model version in order to manage the inter-hemispheric temperature gradient (see Fasullo and Richter (2023) for details and for a discussion of differences with CESM1).

Fig. 2f and 2g, together with Fig. 1g and 1h further inform whether the achieved cooling is linear with respect to increasing injection rates. Fig. 2g indicates that in the three scenarios the injection rates and produced AOD are proportional, but the coefficient of the linear fit between the three is different because of dynamics in the first part (higher injections in the first years mean that AOD needs some years before it converges) and because of microphysical nonlinearities in the second. Therefore, if one only had the SAI-1.5 simulation, and assumed linearity and excluded the first 10 years as SO_2 to AOD converges, they would conclude that it would take 24 Tg-SO_2 to achieve a global AOD of 0.3, whereas in SAI-0.5 it takes 26, an 8% error. Similarly, Fig. 1h and Fig. 2g show that the same unit of AOD results in a slightly different amount of cooling: 6 K per unit of AOD globally, in SAI-1.5, and 7 in SAI–0.5), a 14% difference. Overall, both sub-linearities

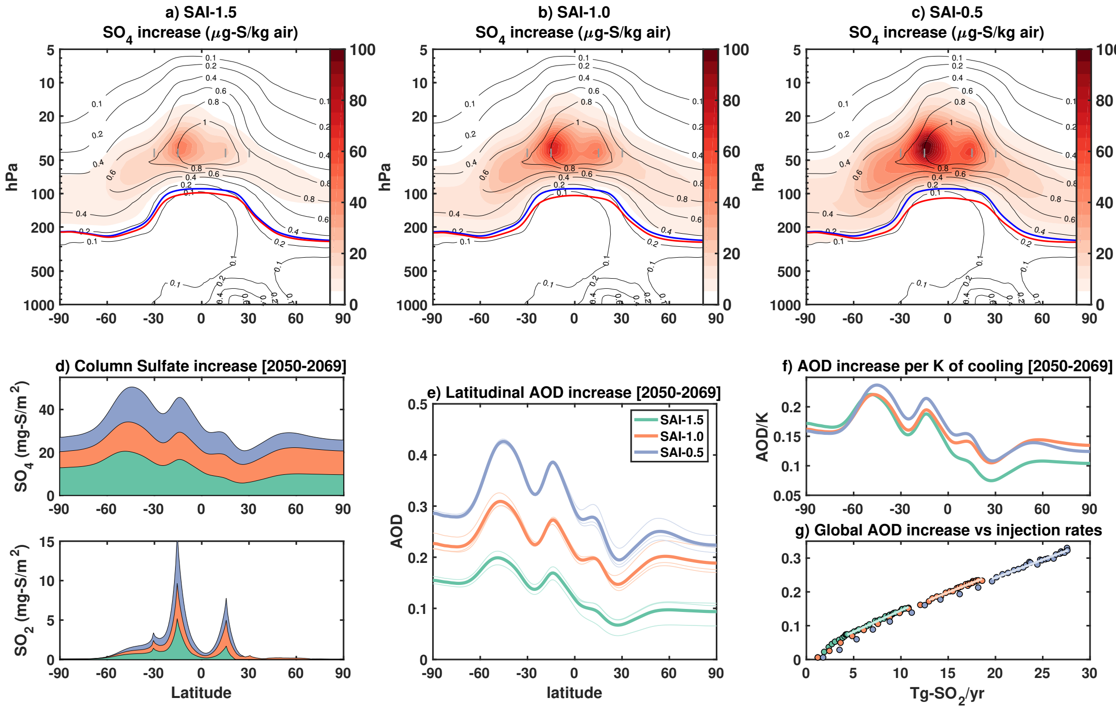

Figure 2. a-c) Shading: Zonal mean increase in sulfate mass concentrations (in ug-S/kg-air) for the 2050-2069 period in the three SAI experiments (SAI-1.5, SAI-1.0 and SAI-0.5 compared to the 2020-2039 period in the background SSP2 simulation (shown as thin contour lines). Blue line indicates the average annual tropopause height in the background SSP2 simulation for the 2020-2039 period, red lines indicate the same quantity for the three respective SAI simulations over 2050-2069. d) Zonal mean increase in the overall column burden in the three simulations for SO4 (top) and SO_2 (bottom) for 2050-2069. e) Zonal mean stratospheric optical depth (sOD) increase for 2050-2069, lighter lines show single ensemble realizations. f) Zonal mean increase in stratospheric optical depth (sAOD) normalized by the resulting cooling over the same period. g) global mean AOD as a function of SO_2 injected in the same year.

compound in those found in Fig. 1g and discussed in Section 2.3, resulting in a 31% error in estimating the required injection to achieve the cooling in SAI-0.5 based on the SAI-1.5 simulations.

3.2 Temperature response

An important question when discussing the possible surface response to SAI is "What should simulations of SAI be compared against?". We offer as an example one previous comparison available in the literature: the GeoMIP G6sulfur simulation protocol (Kravitz et al., 2015). This simulation protocol used a scenario following the SSP5-8.5 emissions and prescribed an intervention where SAI was applied to bring temperatures down to those in a scenario following theSSP2-4.5 emissions. For a future period simulated with SAI, one could thus compare a certain quantity (mean temperature, mean precipitation, frequency or intensity of a type of extreme event) against both SSP5-8.5 and SSP2-4.5 and observe which spatial differences are present in G6sulfur minus SSP2-4.5, and contrast them with those between SSP5-8.5 and SSP2-4.5.

In our case, our set of simulations can help us expand this comparison by being more explicit on what our goals are. The central problem with GHG-induced global warming (as a measure of other changes) is that it shifts the climatic state outside of historical climate variability, it does so too fast for ecosystems and human adaptation capabilities, and it risks approaching irreversible changes in the system (i.e. tipping points, Lenton et al. (2008)). The comparison of a future (SSP2-4.5) and past period helps identify these changes, with different future GHG concentration levels dictating the amount of warming (Meinshausen et al. (2020), not shown here). SAI introduces a new dimension, as the stratospheric aerosol cooling, on top of increasing GHG concentrations, can reduce the increase of global mean temperatures, stop it, or even cool down to a previous level compared to present days. Evaluations of the SAI+GHG scenarios can thus compare them against:

1. Future periods without SAI, but with the same GHG concentrations (and higher global temperatures), which which is relevant for comparative impact assessment.
2. Present day period, hence with lower GHG concentrations, which highlights differences with currently experienced climate by highlighting "deviations" from a (somewhat arbitrarily chosen) baseline state, though deviations from this state do not directly convey information about impacts.
3. Periods with same global mean temperature, but lower GHG concentrations (with the same caveats). Depending on the SAI scenarios, some of these periods might overlap or hold different meanings: in the G6sulfur example, (3) also indicates a future period, but with less warming because of the underlying SSP scenario, and "present day" is cooler than both.

In the cases under analyses here, SAI-1.5 cools by construction exactly at the "present day" level (2020-2039), while SAI-1.0 and SAI-0.5 cool further, allowing for a three point comparison between SSP2-4.5, SAI and baseline cases. Finally, instead of selecting just one "baseline" with a strict comparison of periods with the same global mean temperature, one can compare against a larger portion of the historical period, focusing on understanding when the compensation of GHG warming with SAI cooling results in a state that lies in a certain range of historical variability.

Examples of comparisons as outlined above are given in Figure 3 for the spatial distribution of temperature changes in the last 20 years of simulation. Top row panels show the regional effects of global temperature warming under SSP2-4.5 by comparing the future period with present or past periods with lower global mean temperature. Comparing SSP2-4.5 with 'present day' (2020-2039, BASE-1.5) already shows changes detectable everywhere on the globe, with a global average increase of 1.3 ºC. By comparing the same time period in the SAI-1.5 simulation against this reference, we can observe how "effective" our simulated SAI strategy is in offsetting the GHG-induced warming. Using a double-sided t-test to determine statistical significance at a 95% level, temperature changes would be detectable only in 27% of the world compared to BASE-1.5. As the 1.5 ºC threshold is, in many ways, arbitrary, one can also choose to compare against other periods, such as when temperatures were cooler, e.g. the 2008-2027 (BASE-1.0) and 1993-2012 (BASE-0.5). If SAI only cools globally by 0.8 ºC (as in the SAI-1.5 simulation), then most areas will still be warmer than 0.5ºC above PI. A similar statement can be made for the other simulations and other possible reference periods. In Fig. 3 we highlight this aspect by representing the overall space of possible comparisons using a matrix approach in which rows represent any future simulation (either SSP2-4.5, SAI-1.5, SAI-1.0 or SAI-0.5) and the columns represent a potential target to compare our future simulation against.

The diagonal panels in Fig. 3 show changes in SAI-1.5, SAI-1.0 and SAI-0.5 against their target periods, BASE-1.5, BASE-1.0 and BASE-0.5 (i.e. the periods in the past with the same 20-year-mean global mean temperature). This comparison highlights that more cooling results in more areas that show statistically significant temperature changes. Among these changes is a temperature increase over the Eastern Pacific, projecting onto the pattern associated with the positive phase of the El-Nino Southern Oscillation (ENSO), and a temperature decrease over the Northern Atlantic, indicating a weakening of the At-

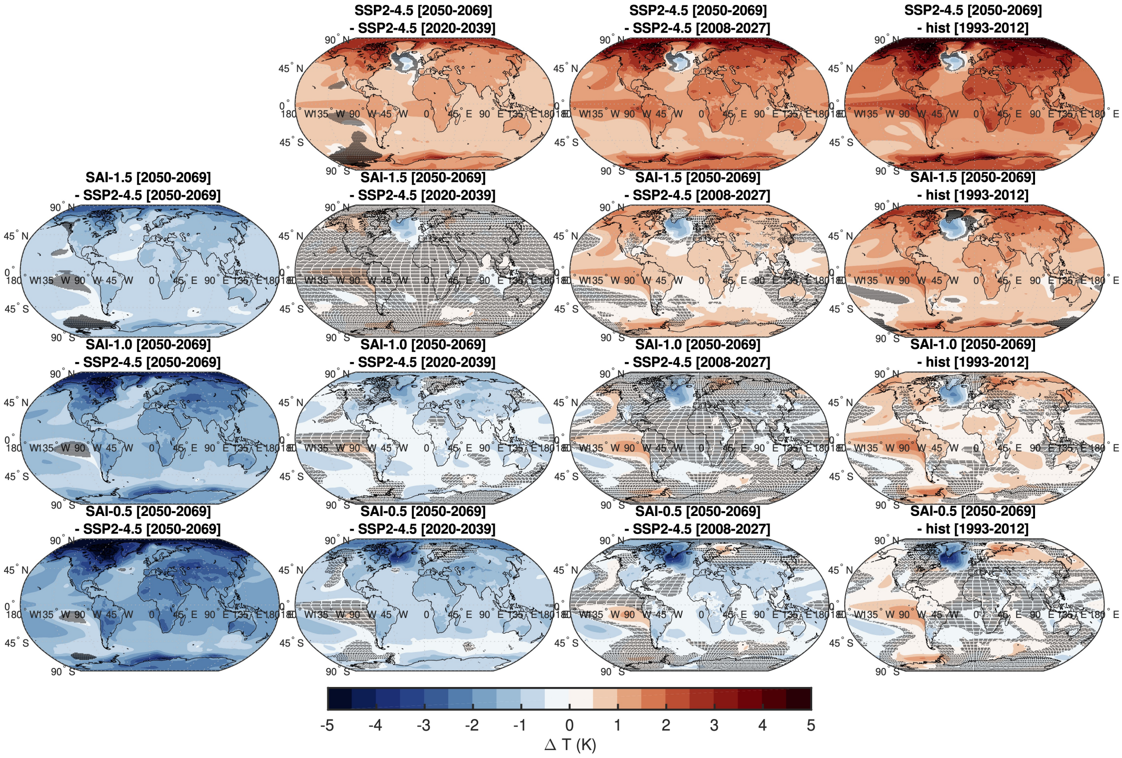

Figure 3. Comparison of surface temperatures changes averaged over 20 years periods and all ensemble members. The rows indicate the first term of the comparison, while the columns indicate the second. SSP2-4.5 [2050-2069] is both the first row and first column, indicating the reference future with an increase in CO_2 concentrations that is unabated by SAI. The other three rows show the three SAI simulations, from the one cooling the least (SAI-1.5) to the one cooling the most (SAI-0.5). The other three columns indicate the reference period selected, from the future to the historical period [1993-2012] (as simulated in CESM2-WACCM6).

lantic Meridional Overturning Circulation (AMOC). Both of these responses are analyzed in more depth in Sections 3.2.1 and 3.3. Items of comparison outside of the diagonal in Fig. 3 also offer valuable information. For instance, the comparison between SAI-1.5 and SSP2-4.5 (second row, third column) shows the results in which warming between SSP2-4.5 in 2050-2069 and BASE-1.0 (which equates to a 1.5ºC temperature difference) is halved rather than considering it as an SAI case in which the whole warming from the period 2020-2039 is offset. In this case, one could argue that the cooling produced is moderate (P. Irvine et al., 2019; P. J. Irvine & Keith, 2020) (i.e. it doesn't offset the whole amount of warming) and thus would incur less SAI-induced changes (albeit most areas in such a strategy, by definition, would still be warmer than the period under comparison).

In general, we highlight that the particular choice of a baseline period can yield different results, speficically in the perceptual sense of discussing if a particular feature looks "better" or "worse" under SAI, and while having a context in which to understand mechanistic changes to climatic features is important (as we will discuss in the following sections), it might always result in biased assessments of the role of SAI (Reynolds, 2022). It is crucial therefore to think of better ways to interpret changes due to SAI to make sure future assessments are more meaningful.

3.2.1 Eastern tropical Pacific response

El Niño/Southern Oscillation (ENSO) is one of the main climatic modes of variability, the teleconnections of which have worldwide impacts (Timmermann et al., 2018). During El Niño periods an anomalous sea surface temperature (SST) warming pattern can be identified in the eastern/central Pacific, replaced by an anomalous SST cooling pattern during La Niña. These anomalies in the Pacific sea-surface temperatures are strongly coupled to changes in atmospheric convection and Walker Circulation, thereby affecting weather patterns on both sides of the Pacific Ocean. ENSO is a complex and highly variable phenomenon, and understanding its changes and impacts requires a detailed representation of a complex interplay of ocean and atmospheric processes.

Under GHG-induced warming, an increased equatorial Pacific warming and a weakening of the Walker circulation (Vecchi et al., 2006) are projected to lead to a stronger ENSO magnitude and frequency (Cai et al., 2015); this has been inferred through ENSO proxies (Grothe et al., 2020), reanalyses and multi-model projections (Cai et al., 2021). Given the need for long simulations in order to properly sample the underlying processes, provided the high variability and a comparatively long period of an average ENSO cycle, few results are available for SRM simulations. (Gabriel & Robock, 2015) examined a range of different GeoMIP G1-G4 experiments and found no statistically robust changes in ENSO characteristics under geoengineering compared to those driven by the GHGs alone. (Malik et al., 2020) used a 1000-year-long solar dimming simulation to assess changes in the mean state and extreme ENSO events, and found some significant changes compared to preindustrial. Such changes were, however, in large part driven by the tropical overcooling typical of solar dimming simulations (Visioni, MacMartin, & Kravitz, 2021) and would thus not be representative of more complex SAI strategies maintaining multiple surface temperature gradients such as those analyzed here.

In the absence of SAI, the simulated (20-year mean) SST pattern in the Pacific Ocean is similar to the positive phase of ENSO, (Fig. 3, first row), potentially due to similar mechanisms as the projected intensification of the El- Niño events under GHG-induced warming and the weakening of the Walker Circulation (see Section 3.4.1, Fig. 7) . Despite the cancellation of the global mean surface temperature increase under SAI, when the different SAI scenarios are compared against each individual baseline period the simulations still show increased SST in the eastern Pacific, suggestive also of a mean response with a pattern similar to the positive phase of ENSO that is not compensated by the SAI global cooling, statistically significant for SAI-1.0 and SAI-0.5 (diagonal maps in Fig. 3).

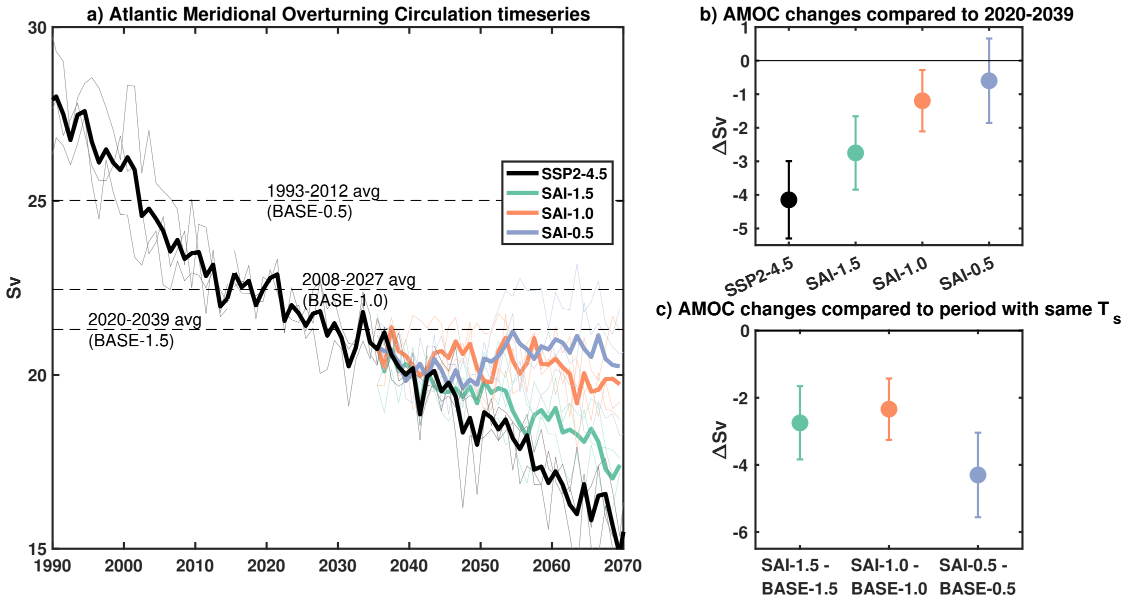

Figure 4. a) Yearly mean values of AMOC strength in all simulations, defined as the maximum value of the North Atlantic meridional overturning streamfunction. Lighter lines indicate single ensemble realizations, while thicker lines indicate the ensemble average. b) Changes in AMOC strength in 2050-2069 compared to the values in the period 2020-2039. The error bars indicate ±1 standard error of the difference in means. c) Changes in AMOC strength in 2050-2069 for the three SAI simulations compared to their respective period with the same global mean surface temperature.

3.3 AMOC response

Fig. 4a shows a timeseries of the simulated AMOC strength, while Fig. 4b shows the associated twenty year average changes in 2050-2069 compared against the same quasi-present day BASE1.5 period and Fig. 4c shows the twenty year changes compared against each individual baseline period. In the absence of SAI, the strength of AMOC decreases under SSP2-4.5 because of the polar amplification and the resulting weakening of the temperature and salinity vertical gradients in the Northern Atlantic (Fasullo et al., 2018; Fasullo & Richter, 2023).

We find that all SAI scenarios slow AMOC weakening, with the effectiveness increasing marginally under increased magnitude of SAI. Importantly, the differences in the AMOC response among the three different SAI scenarios, when compared against the same BASE1.5 baseline period, are much smaller than the long-term GHG-induced AMOC trend under SSP2-4.5 alone when compared against the three different baseline periods. Thus, if one chooses to compare the SAI AMOC responses against their respective baseline periods the results show increased weakening under increased magnitude of SAI. In contrast, comparing the SAI AMOC responses against the same quasi-present day baseline period the results show reduced weakening under increased magnitude of SAI. This inconsistency is primarily driven by the differences in AMOC strength during the different reference periods, i.e. before SAI started. This analysis is another example presented here which highlights the importance of the chosen baseline period when evaluating the SAI responses under different magnitudes of global cooling.

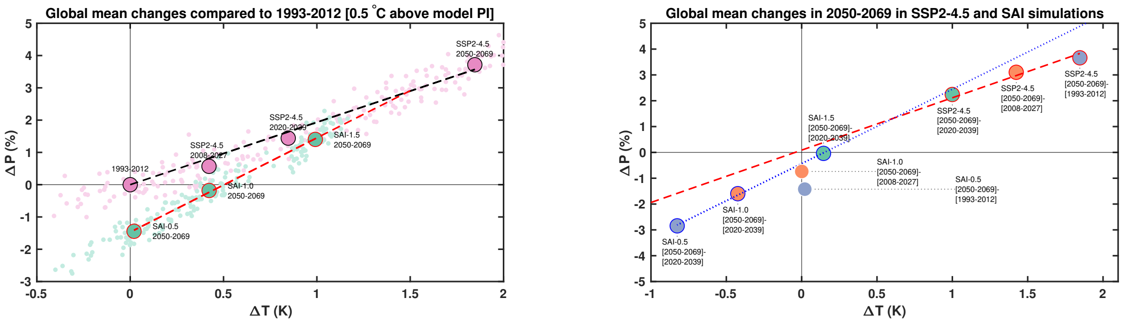

Figure 5. Changes in global mean temperature (K) compared to changes in precipitation (as a percent of the baseline precipitation, %), representing the Hydrological Sensitivity to both GHG-induced warming and SAI-induced cooling. In panel a), the values are represented against the coldest period analyzed in this work (1993-2012, 0.5ºC above PI), for all three warmer periods due to GHG (2008-2027 for 1.0ºC above PI; 2020-2039 for 1.5ºC above PI; and 2050-2060 for 2.4ºC above PI) and for the three SAI simulations in the period 2050-2069 with the three different levels of cooling. The single yearly values for each period and all ensemble members are also shown. In panel b), SAI values in 2050-2069 are compared against the 2020-2039 reference period, while the SSP2-4.5 values in 2050-2069 are compared against time periods which represent cooler temperatures in SSP2-4.5 in increments of0.5ºC.

3.4 Precipitation response

The precipitation response to changes in temperature has been previously investigated both for GHG-induced warming and for simulated SAI cooling . For abrupt 4xCO_2 experiments in the literature, this response can be typically divided into a fast (cloud, vegetation and radiative response to the perturbation) and a slow (usually identified with a temperature-driven response) contribution (Tilmes et al., 2013; Cao et al., 2015).

Under long-term changes in tropospheric temperatures, global mean precipitation tends to scale linearly with the surface temperatures. This relationship (called hydrological sensitivity, HS) can be explained in terms of changes to the energy balance of the atmosphere, and is a combination of the fast and slow response described above (Held & Soden, 2006; Pendergrass & Hartmann, 2014). The linearity of this response has been shown to hold in both modeling studies (Kvalevåg et al., 2013) and observational studies (DelSole et al., 2016), but with spread between individual models (Fläschner et al., 2016) and with considerable uncertainties over the available measurements (DelSole et al., 2016). In general, for the GHG-induced warming, the modeling consensus lies around 2-3% precipitation increase per 1 K of warming (Samset et al., 2018). For CESM, this is confirmed in Fig. 5 where we show a HS of 2.0% increase per K of warming in SSP2-4.5 as compared to the three reference periods with 1.5, 1.0 and 0.5 ºC above the model PI.

For SRM, multiple modeling studies reported that for a certain amount of cooling, global precipitation would be reduced more compared to a GHG-induced increase (Niemeier et al., 2013; Tilmes et al., 2013), leading to what is usually termed as an "overcompensation of precipitation versus temperature". Thermodynamical changes in the vertical temperature gradient is shown to be one of the reasons behind this, as the forcing from elevated CO_2 cannot be perfectly matched by a reduction in the incoming solar radiation, due to different mechanisms as the former warms from the bottom-up, and the latter cools from the top-down (Govindasamy et al., 2003; Ricke et al., 2023). Other reasons include the contribution of the aerosol-induced stratospheric heating under SAI (Simpson

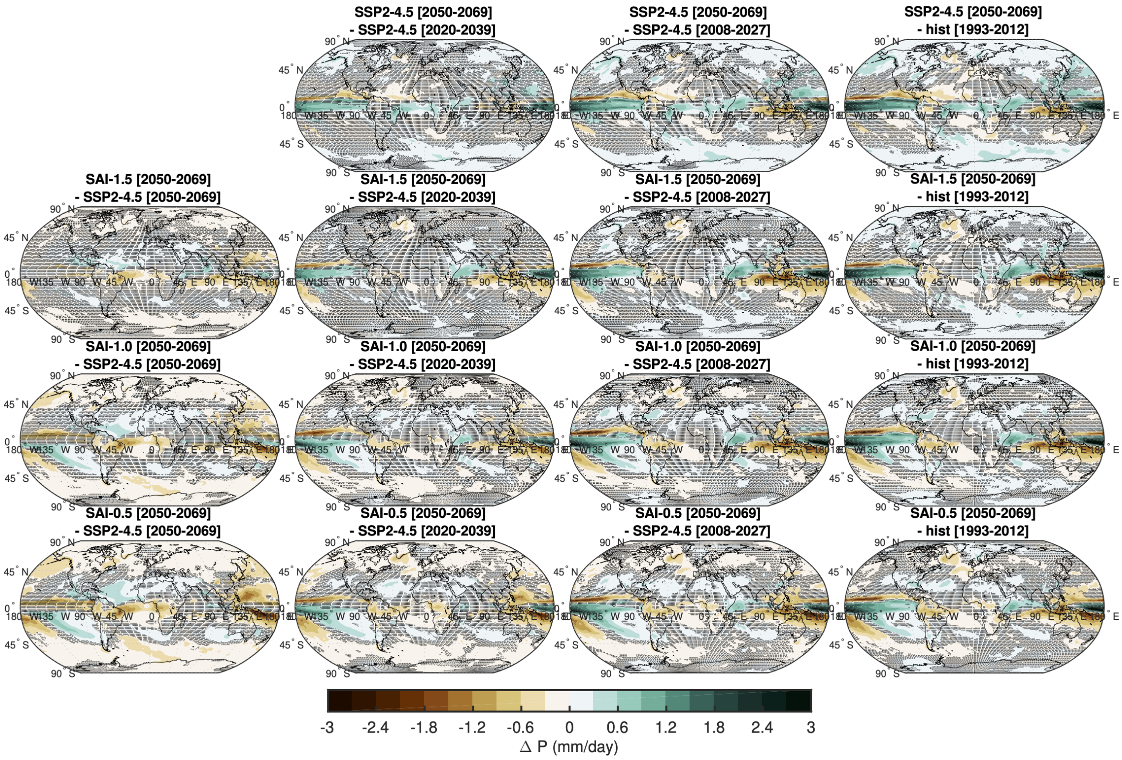

Figure 6. As in Fig. 3, but for the yearly mean precipitation response (mm/day).

et al., 2019; Visioni, MacMartin, & Kravitz, 2021) or differences between the land response to shortwave versus longwave forcing (Niemeier et al., 2013). As shown in Fig. 5, the SRM-specific changes are also confirmed in our simulations with different levels of cooling as the slope of the linear fit for the SAI simulations when compared to the same reference period (2020-2039) is steeper than the warming-derived one (2.9% decrease per K of cooling). Similarly, when the SAI simulations are compared against their respective baseline periods the difference between the two slopes is also evident. In these cases, the data points for SAI-1.0 vs BASE-1.0 and SAI-0.5 vs BASE-0.5 indicate, by definition, no changes in the global mean surface temperature; yet, the corresponding reduction in the global mean precipitation grows larger with increasing levels of SAI. This change in hydrological sensitivity induced by the compensation of GHG-warming with SAI can be estimated to be equivalent to a 0.9% decrease per SAI-induced cooling.

3.4.1 Regional changes

Regionally, precipitation changes will reflect modulations of the large-scale tropospheric circulation patterns. At this spatial scale, these changes are driven by the position and intensity of the Hadley (including the behavior of the Intertropical Convergence Zone, ITCZ) and Walker Circulations as well as monsoonal circulation due to the different temperature response between land (which warms or cools faster) and ocean.

The SSP2-4.5 precipitation response largely reflects the southward shift of the ITCZ (Fig. S2) due to different rates of warming between the hemispheres, potentially also driven by different tropospheric aerosol emissions (cite), alongside the overall increase in the global mean precipitation caused by the increase in the global mean surface temperatures. The combination of these two factors leads to an increase in yearly mean precipitation in equatorial Africa (Fig. 6). In the eastern Indian and western Pacific Ocean regions, the weakening and eastward shift of the Walker Circulation in SSP2-4.5 (Fig. 7)

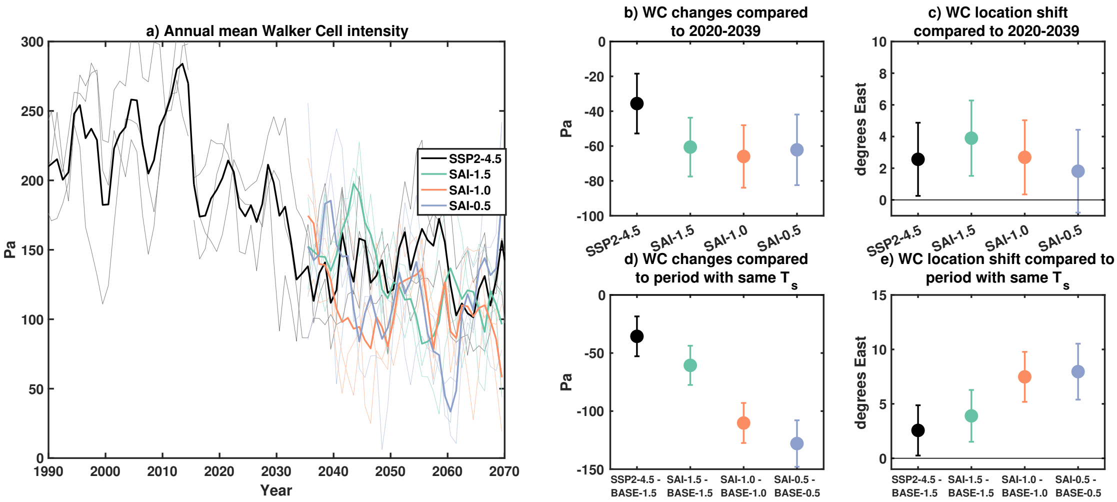

Figure 7. a) Annual mean Walker Circulation (WC) intensity for all experiments, with a 5-year moving average. b) Annual mean changes in the WC intensity from 2050-2069 compared to 2020-2039, and c) annual mean changes in the location of the transition between the anticlockwise and the clockwise cells over the Indian Ocean and Western Pacific for the same time periods. d) Annual mean changes in the WC intensity for the three SAI simulations compared to each respective time period with the same global mean surface temperature, and e) annual mean changes in the location of the transition between the anticlockwise and the clockwise cells over the Indian Ocean and Western Pacific for the same time periods. The intensity of the Walker circulation is calculated using the SLP-base method (see text for details). The error bars indicate ±1 standard error of the difference in means.

initiates a reduction in precipitation in the Indonesian region. We use two metrics of the Walker Circulation: i) a pressure based index of its intensity, defined as the difference in sea level pressure between east/central Pacific (160W-80W, 5S-5N) and western Pacific (80-160E, 5S-5N), as in Kang et al. (2020); and ii) the location of the individual cells of the Walker Circulation, estimated from the zonal mass streamfunction. The latter is calculated using the divergent component of zonal wind, averaged over 10S-10N, following the formula in (Guo et al., 2018). The longitudinal shift of the Walker Circulation is approximated by the shift of the zero line in the stream function at 400 hPa over the Indian Ocean and Western Pacific (80E-200E).

The weakening and eastward shift of Walker Circulation has been commonly simulated in climate models as a result of rising greenhouse gas levels and, thus, changes in static stability and lapse rate brought about by upper tropospheric temperature changes (e.g. Bayr et al. (2014); Nowack et al. (2015)). The weakening of the Walker Circulation under global warming is also consistent with the projected intensification of the El-Niño like events discussed in Section 3.2.1.

As discussed in Section 3.4, no significant change to global mean precipitation is simulated in SAI-1.5 (compared to 2020-2039), and the small decreases in SAI-1.0 and SAI-0.5 is due to the associated decreases in the global mean temperatures (Fig. 5). Regarding the ITCZ position, the use of the feedback algorithm controlling the interhemispheric temperature gradient (T1) reduces the magnitude of the ITCZ shift in the SAI simulations compared to SSP2-4.5 (Fig. S2). Yet, a small ITCZ shift is nonetheless found in all SAI simulations illustrating that the feedback control over T1 is not a sufficient constraint. The magnitude of the ITCZ shift is however similar among the three SAI scenarios.

Aside from the thermodynamically-driven changes in global mean precipitation and those arising from shifts in the tropical zonal mean circulation and ITCZ, the SAI simulations also show relevant changes to the tropical Walker Circulation (Fig. 7). In particular, all three SAI simulations show a weakening and an eastward shift of the Walker circulation, the magnitude of which increases with more cooling when the SAI simulations are compared against their respective baseline period. In contrast, when compared to the same quasi-present day baseline period, the SAI simulations show little change to the strength or position of the Walker Circulation under increasing magnitude of SAI. Notably, the sea-level pressure anomalies in the eastern Pacific strengthen under increasing magnitude of SAI forcing but the anomalies in the western Pacific weaken(Fig. S4). This result leads to similar changes of the Walker Circulation intensity across the three SAI scenarios in Fig. 7 and suggests that factors other than global mean temperature contribute to the Walker Circulation and precipitation response in the region under SAI. The contrasting behavior which is dependent upon the baseline period likely reflects the contribution of the GHG-induced changes in the Walker Circulation during the period before SAI is started. These different baseline periods reflect different background (i.e. non-SAI) forcings as shown by the large differences in the SSP2-4.5 responses as compared to its temperature-dependent baseline periods (Fig. 7 and S3). This result highlights the importance of considering the baseline period when interpreting SAI impact on Walker Circulation.

4 Conclusions

In this work, we presented results from multiple sets of Stratospheric Aerosol Injection (SAI) simulations in which SO_2 injections at four different latitudes are used to maintain annual and global mean surface temperatures at 1.5, 1.0 and 0.5 ^{o}C above preindustrial (PI) levels (SAI-1.5, SAI-1.0 and SAI-0.5 respectively) while greenhouse gas emissions follow the CMIP6 SSP2-4.5 scenario.

The analyses serve to better understand the linearity of the climate response to the different magnitudes of SAI. Furthermore, this work can help inform the design of an emulator to be used to analyze comparatively large sets of SAI scenarios that would not be computationally feasible using a fully-coupled Earth system model.

The three SAI scenarios all start SO_2 injections in 2035 and continue through 2069, with analyses focusing on the last 20 years (2050-2069). For each of these SAI scenarios, a corresponding 20-year-long baseline period is established from the SSP2-4.5 and/or historical simulation (without SAI) that has the same global mean temperature: 2020-2039 for SAI-1.5, 2008-2027 for SAI-1.0 and 1993-2012 for SAI-0.5. The choice of this baseline period with the same global mean surface temperature permits an evaluation of the diverse distribution of impacts arising from the imperfect compensation of the GHG-induced warming with the cooling produced by the sulfate. Additionally, comparing the SAI simulations against the same future period from the reference SSP2-4.5 scenario without SAI facilitates an evaluation of the direct effectiveness of SAI compared to a future climate modified by the GHG-induced warming. Finally, a comparison of the SAI scenarios and their impacts against the present day baseline period (here taken as 2020-2039) provides valuable information for future SAI decision making processes. In addition to stressing the importance of the choice of baseline period has for the context of the discussion, we also presented a couple of examples when the choice of baseline period can spuriously affect the conclusions regarding the effectiveness and linearity of the SAI responses (e.g. on the strength of AMOC or Walker Circulation) under varying magnitudes of the global mean surface cooling.

The main goal behind these simulations and of this work is to illustrate that an evaluation of SAI impacts needs to take into account multiple dimensions in order to highlight trade-offs and properly identify the space of possible SAI-driven impacts (MacMartin et al., 2022). Here we have focused on the amount of cooling that SO_2 is chosen to produce, a method that is similar to the scenario exploration under different GHG concen-

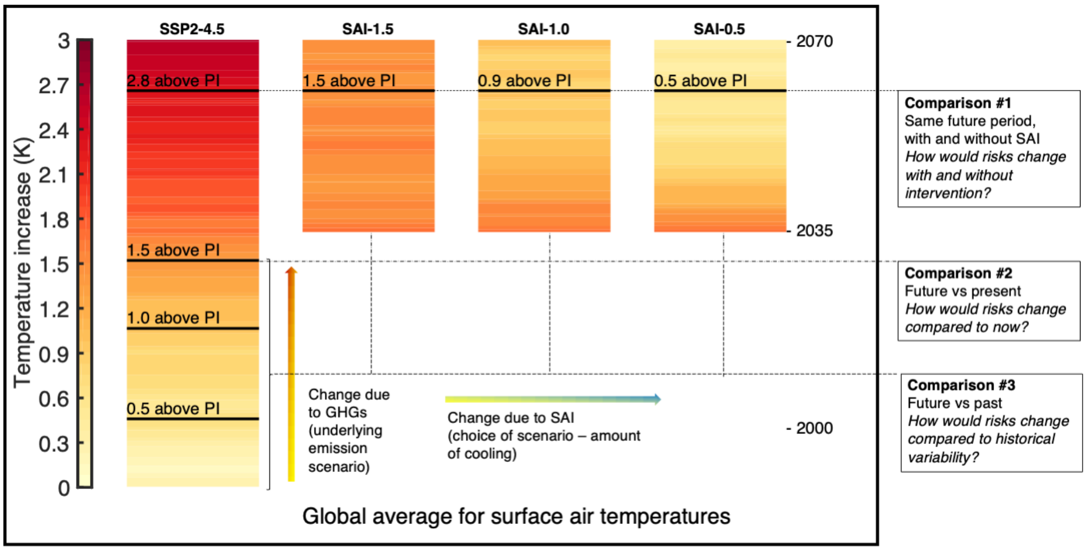

Figure 8. A schematic figure reflecting on the potential choices of comparison periods when discussing SAI impacts. Colorbar indicate global mean, ensemble mean average for surface temperature (K) as a deviation from the PI value.

trations in the IPCC scenarios (Meinshausen et al., 2020). In other works, the way in which some impacts are driven by different SO_2 injection locations (the injection strategy) has been explored (Kravitz et al., 2019; Visioni, MacMartin, Kravitz, Richter, et al., 2020; Bednarz et al., 2023; Zhang et al., 2023). Together these studies provide an overview of the possible design space of SAI that form a foundation for future SAI explorations in a multi-model framework.

This work highlights that SAI studies, by adding a novel dimension to the ability to influence global warming impacts, need even more care when explaining how they are defining a certain simulated impact. Comparisons between different baseline periods can yield different insight onto what constitutes a direct SAI impacts, as opposed to what constitutes an imperfect compensation between GHG-induced warming and SAI: for instance, a change in tropospheric circulation due to stratospheric heating (Simpson et al., 2019; Bednarz et al., 2022) as opposed to the sea-land contrast not restored due to different heat capacities resulting in monsoonal circulation changes (Visioni, MacMartin, Kravitz, Richter, et al., 2020). While such comparisons are fundamental for determining some of the physical drivers (and thereby, might warrant SAI simulations with higher signal-to-noise ratio), it is hard to capture the nuance when discussing potential impacts and risks from a policy-relevant perspective. The choice of reference period is also relevant because people will interpret such comparison plots to infer influences on climate impacts, e.g., noting that some precipitation or temperature feature is over- or under-compensated relative to the compensation of global mean temperature; that SAI creates a "novel" climate state. In this sense, though, any choice of current or historical reference period is potentially misleading: if some climate variable is restored to levels consistent with the past period when global mean temperature was 1.5ºC above preindustrial, and some other variable restored to levels consistent with an earlier historical period when global mean temperature was 1.0ºC, it is entirely unobvious what the influence of that novel climate state would have on human or ecosystem impacts, and the answer would depend on what changes have already been adapted to, for example. For this reason, it is important to stress that there is no single reference period relevant for inferring ultimate impacts and indeed it may be more appropriate to compare to a range of past conditions rather than to any single state (Figure 8).

5 Open Research

All model output analysed in this work is available at https://doi.org/10.7298/xr82-sv86 (Visioni, 2022).

Acknowledgments

We would like to acknowledge high-performance computing support from Cheyenne (https://doi.org/10.5065/D6RX99HX) provided by NCAR's Computational and Information Systems Laboratory, sponsored by the National Science Foundation. Support was provided by the NOAA cooperative agreement NA22OAR4320151, NOAA Earth's Radiative Budget initiative, Cornell Atkinson Center for Sustainability, and by the National Science Foundation through agreement CBET-2038246. Support for BK was provided in part by the National Science Foundation through agreement SES-1754740 and the Indiana University Environmental Resilience Institute. The Pacific Northwest National Laboratory is operated for the US Department of Energy by Battelle Memorial Institute under contract DE-AC05-76RL01830.

References

Ban-Weiss, G. A., & Caldeira, K. (2010). Geoengineering as an optimization problem. *Environmental Research Letters*, *5*(3). doi: 10.1088/1748-9326/5/3/034009

Bayr, T., Dommenget, D., Martin, T., & Power, S. B. (2014, November). The eastward shift of the Walker Circulation in response to global warming and its relationship to ENSO variability. *Climate Dynamics*, *43*(9), 2747–2763. Retrieved from `https://doi.org/10.1007/s00382-014-2091-y` doi: 10.1007/s00382-014-2091-y

Bednarz, E. M., Butler, A. H., Visioni, D., Zhang, Y., Kravitz, B., & MacMartin, D. G. (2023). Injection strategy – a driver of atmospheric circulation and ozone response to stratospheric aerosol geoengineering. *EGUsphere*, *2023*, 1–32. Retrieved from `https://egusphere.copernicus.org/preprints/2023/egusphere-2023-495/` doi: 10.5194/egusphere-2023-495

Bednarz, E. M., Visioni, D., Richter, J. H., Butler, A. H., & MacMartin, D. G. (2022). Impact of the latitude of stratospheric aerosol injection on the southern annular mode. *Geophysical Research Letters*, *49*(19), e2022GL100353. Retrieved from `https://agupubs.onlinelibrary.wiley.com/doi/abs/10.1029/2022GL100353` (e2022GL100353 2022GL100353) doi: https://doi.org/10.1029/2022GL100353

Boettcher, M., Brent, K., Buck, H. J., Low, S., McLaren, D., & Mengis, N. (2021). Navigating potential hype and opportunity in governing marine carbon removal. *Frontiers in Climate*, *3*. Retrieved from `https://www.frontiersin.org/articles/10.3389/fclim.2021.664456` doi: 10.3389/fclim.2021.664456

Brecha, R. J., Ganti, G., Lamboll, R. D., Nicholls, Z., Hare, B., Lewis, J., . . . Gidden, M. J. (2022, August). Institutional decarbonization scenarios evaluated against the Paris Agreement 1.5 °C goal. *Nature Communications*, *13*(1), 4304. Retrieved from `https://doi.org/10.1038/s41467-022-31734-1` doi: 10.1038/s41467-022-31734-1

Cai, W., Santoso, A., Collins, M., Dewitte, B., Karamperidou, C., Kug, J.-S., . . . Zhong, W. (2021, September). Changing El Niño–Southern Oscillation in a warming climate. *Nature Reviews Earth & Environment*, *2*(9), 628–

644. Retrieved from https://doi.org/10.1038/s43017-021-00199-z doi: 10.1038/s43017-021-00199-z

Cai, W., Santoso, A., Wang, G., Yeh, S.-W., An, S.-I., Cobb, K. M., … Wu, L. (2015, September). ENSO and greenhouse warming. *Nature Climate Change*, *5*(9), 849–859. Retrieved from https://doi.org/10.1038/nclimate2743 doi: 10.1038/nclimate2743

Cao, L., Bala, G., Zheng, M., & Caldeira, K. (2015, December). Fast and slow climate responses to CO2 and solar forcing: A linear multivariate regression model characterizing transient climate change. *Journal of Geophysical Research: Atmospheres*, *120*(23), 12,037–12,053. Retrieved 2023-05-24, from https://doi.org/10.1002/2015JD023901 (Publisher: John Wiley & Sons, Ltd) doi: 10.1002/2015JD023901

Crutzen, P. J. (2006). Albedo enhancement by stratospheric sulfur injections: A contribution to resolve a policy dilemma? *Climatic Change*, *77*(3), 211–220. Retrieved from https://doi.org/10.1007/s10584-006-9101-y doi: 10.1007/s10584-006-9101-y

Danabasoglu, G., Lamarque, J.-F., Bacmeister, J., Bailey, D. A., DuVivier, A. K., Edwards, J., … Strand, W. G. (2020). The Community Earth System Model Version 2 (CESM2). *Journal of Advances in Modeling Earth Systems*, *12*(2), e2019MS001916. doi: https://doi.org/10.1029/2019MS001916

Davis, N. A., Visioni, D., Garcia, R. R., Kinnison, D. E., Marsh, D. R., Mills, M. J., … Vitt, F. (2022, dec). Climate, variability, and climate sensitivity of "middle atmosphere" chemistry configurations of the community earth system model version 2, whole atmosphere community climate model version 6 (CESM2(WACCM6)). Retrieved from https://doi.org/10.22541\%2Fessoar.167117634.40175082\%2Fv1 doi: 10.22541/essoar.167117634.40175082/v1

DelSole, T., Yan, X., & Tippett, M. K. (2016, September). Inferring Aerosol Cooling from Hydrological Sensitivity. *Journal of Climate*, *29*(17), 6167–6178. Retrieved from https://journals.ametsoc.org/view/journals/clim/29/17/jcli-d-15-0364.1.xml (Place: Boston MA, USA Publisher: American Meteorological Society) doi: 10.1175/JCLI-D-15-0364.1

Fasullo, J. T., & Richter, J. H. (2023). Dependence of strategic solar climate intervention on background scenario and model physics. *Atmospheric Chemistry and Physics*, *23*(1), 163–182. Retrieved from https://acp.copernicus.org/articles/23/163/2023/ doi: 10.5194/acp-23-163-2023

Fasullo, J. T., Simpson, I. R., Kravitz, B., Tilmes, S., Richter, J. H., MacMartin, D. G., & Mills, M. J. (2018). Persistent polar ocean warming in a strategically geoengineered climate. *Nature Geoscience*, *11*(12), 910–914. Retrieved from http://dx.doi.org/10.1038/s41561-018-0249-7 doi: 10.1038/s41561-018-0249-7

Fläschner, D., Mauritsen, T., & Stevens, B. (2016, January). Understanding the Intermodel Spread in Global-Mean Hydrological Sensitivity. *Journal of Climate*, *29*(2), 801–817. Retrieved from https://journals.ametsoc.org/view/journals/clim/29/2/jcli-d-15-0351.1.xml (Place: Boston MA, USA Publisher: American Meteorological Society) doi: 10.1175/JCLI-D-15-0351.1

Gabriel, C. J., & Robock, A. (2015). Stratospheric geoengineering impacts on El Niño/Southern Oscillation. *Atmospheric Chemistry and Physics*, *15*(20), 11949–11966. Retrieved from https://acp.copernicus.org/articles/15/11949/2015/ doi: 10.5194/acp-15-11949-2015

Gao, Y., Gao, X., & Zhang, X. (2017). The 2 °c global temperature target and the evolution of the long-term goal of addressing climate change— from the united nations framework convention on climate change to the paris agreement. *Engineering*, *3*(2), 272-278. Retrieved from https://www.sciencedirect.com/science/article/pii/S2095809917303077 doi: https://doi.org/10.1016/J.ENG.2017.01.022

Govindasamy, B., Caldeira, K., & Duffy, P. (2003). Geoengineering earth's radiation balance to mitigate climate change from a quadrupling of CO2. *Global and Planetary Change*, *37*(1), 157 - 168. Retrieved from http://www.sciencedirect.com/science/article/pii/S0921818102001959 (Evaluation, Intercomparison and Application of Global Climate Models) doi: https://doi.org/10.1016/S0921-8181(02)00195-9

Grothe, P. R., Cobb, K. M., Liguori, G., Di Lorenzo, E., Capotondi, A., Lu, Y., ... Toth, L. T. (2020, April). Enhanced El Niño–Southern Oscillation Variability in Recent Decades. *Geophysical Research Letters*, *47*(7), e2019GL083906. Retrieved 2023-05-24, from https://doi.org/10.1029/2019GL083906 (Publisher: John Wiley & Sons, Ltd) doi: 10.1029/2019GL083906

Guo, A., Moore, J. C., & Ji, D. (2018). Tropical atmospheric circulation response to the G1 sunshade geoengineering radiative forcing experiment. *Atmospheric Chemistry and Physics*, *18*(12), 8689–8706. Retrieved from https://acp.copernicus.org/articles/18/8689/2018/ doi: 10.5194/acp-18-8689-2018

Haszeldine, R. S., Flude, S., Johnson, G., & Scott, V. (2018). Negative emissions technologies and carbon capture and storage to achieve the paris agreement commitments. *Philosophical Transactions of the Royal Society A: Mathematical, Physical and Engineering Sciences*, *376*(2119), 20160447. Retrieved from https://royalsocietypublishing.org/doi/abs/10.1098/rsta.2016.0447 doi: 10.1098/rsta.2016.0447

Held, I. M., & Soden, B. J. (2006, November). Robust Responses of the Hydrological Cycle to Global Warming. *Journal of Climate*, *19*(21), 5686–5699. Retrieved from https://journals.ametsoc.org/view/journals/clim/19/21/jcli3990.1.xml (Place: Boston MA, USA Publisher: American Meteorological Society) doi: 10.1175/JCLI3990.1

Holz, C., Siegel, L. S., Johnston, E., Jones, A. P., & Sterman, J. (2018, June). Ratcheting ambition to limit warming to 1.5 °C–trade-offs between emission reductions and carbon dioxide removal. *Environmental Research Letters*, *13*(6), 064028. Retrieved from https://dx.doi.org/10.1088/1748-9326/aac0c1 (Publisher: IOP Publishing) doi: 10.1088/1748-9326/aac0c1

Irvine, P., Emanuel, K., He, J., Horowitz, L. W., Vecchi, G., & Keith, D. (2019). Halving warming with idealized solar geoengineering moderates key climate hazards. *Nature Climate Change*, *9*(4), 295–299. Retrieved from http://dx.doi.org/10.1038/s41558-019-0398-8 doi: 10.1038/s41558-019-0398-8

Irvine, P. J., & Keith, D. W. (2020, mar). Halving warming with stratospheric aerosol geoengineering moderates policy-relevant climate hazards. *Environmental Research Letters*, *15*(4), 044011. Retrieved from https://dx.doi.org/10.1088/1748-9326/ab76de doi: 10.1088/1748-9326/ab76de

Irvine, P. J., Sriver, R. L., & Keller, K. (2012, February). Tension between reducing sea-level rise and global warming through solar-radiation management. *Nature Climate Change*, *2*(2), 97–100. Retrieved from https://doi.org/10.1038/nclimate1351 doi: 10.1038/nclimate1351

Kang, S. M., Xie, S.-P., Shin, Y., Kim, H., Hwang, Y.-T., Stuecker, M. F., ... Hawcroft, M. (2020). Walker circulation response to extratropical radiative forcing. *Science Advances*, *6*(47), eabd3021. Retrieved from https://www.science.org/doi/abs/10.1126/sciadv.abd3021 doi: 10.1126/sciadv.abd3021

Kravitz, B., Lamarque, J.-F., Tribbia, J. J., Tilmes, S., Vitt, F., Richter, J. H., ... Mills, M. J. (2017). First Simulations of Designing Stratospheric Sulfate Aerosol Geoengineering to Meet Multiple Simultaneous Climate Objectives. *Journal of Geophysical Research: Atmospheres*, *122*(23), 12,616–12,634. doi: 10.1002/2017jd026874

Kravitz, B., MacMartin, D. G., Tilmes, S., Richter, J. H., Mills, M. J., Cheng, W.,

... Vitt, F. (2019). Comparing surface and stratospheric impacts of geoengineering with different SO2 injection strategies. *Journal of Geophysical Research: Atmospheres*, *124*(14), 7900-7918. Retrieved from https://agupubs.onlinelibrary.wiley.com/doi/abs/10.1029/2019JD030329 doi: 10.1029/2019JD030329

Kravitz, B., Robock, A., Tilmes, S., Boucher, O., English, J. M., Irvine, P. J., ... Watanabe, S. (2015). The geoengineering model intercomparison project phase 6 (GeoMIP6): simulation design and preliminary results. *Geoscientific Model Development*, *8*(10), 3379–3392. Retrieved from https://gmd.copernicus.org/articles/8/3379/2015/ doi: 10.5194/gmd-8-3379-2015

Kriegler, E., Luderer, G., Bauer, N., Baumstark, L., Fujimori, S., Popp, A., ... van Vuuren, D. P. (2018). Pathways limiting warming to 1.5°c: a tale of turning around in no time? *Philosophical Transactions of the Royal Society A: Mathematical, Physical and Engineering Sciences*, *376*(2119), 20160457. Retrieved from https://royalsocietypublishing.org/doi/abs/10.1098/rsta.2016.0457 doi: 10.1098/rsta.2016.0457

Kvalevåg, M. M., Samset, B. H., & Myhre, G. (2013, April). Hydrological sensitivity to greenhouse gases and aerosols in a global climate model. *Geophysical Research Letters*, *40*(7), 1432–1438. Retrieved 2023-05-24, from https://doi.org/10.1002/grl.50318 (Publisher: John Wiley & Sons, Ltd) doi: 10.1002/grl.50318

Laakso, A., Niemeier, U., Visioni, D., Tilmes, S., & Kokkola, H. (2022). Dependency of the impacts of geoengineering on the stratospheric sulfur injection strategy – part 1: Intercomparison of modal and sectional aerosol modules. *Atmospheric Chemistry and Physics*, *22*(1), 93–118.

Lenton, T. M., Held, H., Kriegler, E., Hall, J. W., Lucht, W., Rahmstorf, S., & Schellnhuber, H. J. (2008). Tipping elements in the earth's climate system. *Proceedings of the National Academy of Sciences*, *105*(6), 1786-1793. Retrieved from https://www.pnas.org/doi/abs/10.1073/pnas.0705414105 doi: 10.1073/pnas.0705414105

Liu, X., Ma, P.-L., Wang, H., Tilmes, S., Singh, B., Easter, R. C., ... Rasch, P. J. (2016). Description and evaluation of a new four-mode version of the Modal Aerosol Module (MAM4) within version 5.3 of the Community Atmosphere Model. *Geoscientific Model Development*, *9*(2), 505–522. doi: 10.5194/gmd-9-505-2016

MacMartin, D. G., Kravitz, B., Mills, M. J., Tribbia, J. J., Tilmes, S., Richter, J. H., ... Lamarque, J.-F. (2017). The Climate Response to Stratospheric Aerosol Geoengineering Can Be Tailored Using Multiple Injection Locations. *Journal of Geophysical Research: Atmospheres*, *122*(23), 12,574–12,590. doi: 10.1002/2017jd026868

MacMartin, D. G., Ricke, K. L., & Keith, D. W. (2018). Solar geoengineering as part of an overall strategy for meeting the 1.5°c paris target. *Philosophical Transactions of the Royal Society A: Mathematical, Physical and Engineering Sciences*, *376*(2119), 20160454. Retrieved from https://royalsocietypublishing.org/doi/abs/10.1098/rsta.2016.0454 doi: 10.1098/rsta.2016.0454

MacMartin, D. G., Visioni, D., Kravitz, B., Richter, J., Felgenhauer, T., Lee, W. R., ... Sugiyama, M. (2022). Scenarios for modeling solar radiation modification. *Proceedings of the National Academy of Sciences*, *119*(33), e2202230119. Retrieved from https://www.pnas.org/doi/abs/10.1073/pnas.2202230119 doi: 10.1073/pnas.2202230119

Malik, A., Nowack, P. J., Haigh, J. D., Cao, L., Atique, L., & Plancherel, Y. (2020). Tropical Pacific climate variability under solar geoengineering: impacts on ENSO extremes. *Atmospheric Chemistry and Physics*, *20*(23), 15461–15485.

Retrieved from https://acp.copernicus.org/articles/20/15461/2020/ doi: 10.5194/acp-20-15461-2020

Masson-Delmotte, V., et al. (Eds.). (2018). *Global Warming of 1.5°C: An IPCC Special Report on the impacts of global warming of 1.5°C above pre-industrial levels and related global greenhouse gas emission pathways, in the context of strengthening the global response to the threat of climate change, sustainable development, and efforts to eradicate poverty.* Geneva, Switzerland: World Meteorological Organization. Retrieved from https://www.ipcc.ch/sr15/

Meinshausen, M., Nicholls, Z. R. J., Lewis, J., Gidden, M. J., Vogel, E., Freund, M., ... Wang, R. H. J. (2020). The shared socio-economic pathway (ssp) greenhouse gas concentrations and their extensions to 2500. *Geoscientific Model Development*, *13*(8), 3571–3605. Retrieved from https://gmd.copernicus.org/articles/13/3571/2020/ doi: 10.5194/gmd-13-3571-2020

Niemeier, U., Schmidt, H., Alterskjær, K., & Kristjánsson, J. E. (2013). Solar irradiance reduction via climate engineering: Impact of different techniques on the energy balance and the hydrological cycle. *Journal of Geophysical Research: Atmospheres*, *118*(21), 11,905-11,917. Retrieved from https://agupubs.onlinelibrary.wiley.com/doi/abs/10.1002/2013JD020445 doi: 10.1002/2013JD020445

Niemeier, U., & Timmreck, C. (2015). What is the limit of climate engineering by stratospheric injection of SO2? *Atmospheric Chemistry and Physics*, *15*(16), 9129–9141. Retrieved from https://www.atmos-chem-phys.net/15/9129/2015/ doi: 10.5194/acp-15-9129-2015

Nowack, P. J., Luke Abraham, N., Maycock, A. C., Braesicke, P., Gregory, J. M., Joshi, M. M., ... Pyle, J. A. (2015, January). A large ozone-circulation feedback and its implications for global warming assessments. *Nature Climate Change*, *5*(1), 41–45. Retrieved from https://doi.org/10.1038/nclimate2451 doi: 10.1038/nclimate2451

Pendergrass, A. G., & Hartmann, D. L. (2014, January). The Atmospheric Energy Constraint on Global-Mean Precipitation Change. *Journal of Climate*, *27*(2), 757–768. Retrieved from https://journals.ametsoc.org/view/journals/clim/27/2/jcli-d-13-00163.1.xml (Place: Boston MA, USA Publisher: American Meteorological Society) doi: 10.1175/JCLI-D-13-00163.1

Rajamani, L., & Werksman, J. (2018). The legal character and operational relevance of the paris agreement's temperature goal. *Philosophical Transactions of the Royal Society A: Mathematical, Physical and Engineering Sciences*, *376*(2119), 20160458. Retrieved from https://royalsocietypublishing.org/doi/abs/10.1098/rsta.2016.0458 doi: 10.1098/rsta.2016.0458

Reynolds, J. L. (2022). Communication of solar geoengineering science: Forms, examples, and explanation of skewing. *The Anthropocene Review*, *0*(0), 20530196221095569. Retrieved from https://doi.org/10.1177/20530196221095569 doi: 10.1177/20530196221095569

Ricke, K., Wan, J. S., Saenger, M., & Lutsko, N. J. (2023). Hydrological consequences of solar geoengineering. *Annual Review of Earth and Planetary Sciences*, *51*(1), null. Retrieved from https://doi.org/10.1146/annurev-earth-031920-083456 doi: 10.1146/annurev-earth-031920-083456

Robock, A., Oman, L., & Stenchikov, G. L. (2008). Regional climate responses to geoengineering with tropical and arctic so2 injections. *Journal of Geophysical Research: Atmospheres*, *113*(D16). Retrieved from https://agupubs.onlinelibrary.wiley.com/doi/abs/10.1029/2008JD010050 doi: https://doi.org/10.1029/2008JD010050

Samset, B. H., Myhre, G., Forster, P. M., Hodnebrog, Ø., Andrews, T., Boucher, O., ... Voulgarakis, A. (2018, January). Weak hydrological sensitivity to temperature change over land, independent of climate forcing. *npj Climate and Atmospheric Science*, *1*(1), 20173. Retrieved from https://doi.org/

10.1038/s41612-017-0005-5 doi: 10.1038/s41612-017-0005-5

Simpson, I., Tilmes, S., Richter, J., Kravitz, B., MacMartin, D., Mills, M., ... Pendergrass, A. (2019). The regional hydroclimate response to stratospheric sulfate geoengineering and the role of stratospheric heating. *Journal of Geophysical Research: Atmospheres*, 2019JD031093. Retrieved from https://onlinelibrary.wiley.com/doi/abs/10.1029/2019JD031093 doi: 10.1029/2019JD031093

Tilmes, S., Fasullo, J., Lamarque, J.-F., Marsh, D. R., Mills, M., Alterskjær, K., ... Watanabe, S. (2013). The hydrological impact of geoengineering in the geoengineering model intercomparison project (GeoMIP). *Journal of Geophysical Research: Atmospheres*, *118*(19), 11,036-11,058. Retrieved from https://agupubs.onlinelibrary.wiley.com/doi/abs/10.1002/jgrd.50868 doi: 10.1002/jgrd.50868

Timmermann, A., An, S.-I., Kug, J.-S., Jin, F.-F., Cai, W., Capotondi, A., ... Zhang, X. (2018, July). El Niño–Southern Oscillation complexity. *Nature*, *559*(7715), 535–545. Retrieved from https://doi.org/10.1038/s41586-018-0252-6 doi: 10.1038/s41586-018-0252-6

Vecchi, G. A., Soden, B. J., Wittenberg, A. T., Held, I. M., Leetmaa, A., & Harrison, M. J. (2006, May). Weakening of tropical Pacific atmospheric circulation due to anthropogenic forcing. *Nature*, *441*(7089), 73–76. Retrieved from https://doi.org/10.1038/nature04744 doi: 10.1038/nature04744

Visioni, D. (2022). *Data from: Scenarios for modeling solar radiation modification.* doi: https://doi.org/10.7298/xr82-sv86

Visioni, D., Bednarz, E. M., Lee, W. R., Kravitz, B., Jones, A., Haywood, J. M., & MacMartin, D. G. (2023). Climate response to off-equatorial stratospheric sulfur injections in three earth system models – part 1: Experimental protocols and surface changes. *Atmospheric Chemistry and Physics*, *23*(1), 663–685. Retrieved from https://acp.copernicus.org/articles/23/663/2023/ doi: 10.5194/acp-23-663-2023

Visioni, D., MacMartin, D. G., & Kravitz, B. (2021). Is turning down the sun a good proxy for stratospheric sulfate geoengineering? *Journal of Geophysical Research: Atmospheres*, *126*(5), e2020JD033952. Retrieved from https://agupubs.onlinelibrary.wiley.com/doi/abs/10.1029/2020JD033952 (e2020JD033952 2020JD033952) doi: https://doi.org/10.1029/2020JD033952

Visioni, D., MacMartin, D. G., Kravitz, B., Boucher, O., Jones, A., Lurton, T., ... Tilmes, S. (2021). Identifying the sources of uncertainty in climate model simulations of solar radiation modification with the g6sulfur and g6solar geoengineering model intercomparison project (geomip) simulations. *Atmospheric Chemistry and Physics*, *21*(13), 10039–10063. Retrieved from https://acp.copernicus.org/articles/21/10039/2021/ doi: 10.5194/acp-21-10039-2021

Visioni, D., MacMartin, D. G., Kravitz, B., Lee, W., Simpson, I. R., & Richter, J. H. (2020). Reduced poleward transport due to stratospheric heating under stratospheric aerosols geoengineering. *Geophysical Research Letters*, *n/a*(n/a), e2020GL089470. Retrieved from https://agupubs.onlinelibrary.wiley.com/doi/abs/10.1029/2020GL089470 (e2020GL089470 2020GL089470) doi: 10.1029/2020GL089470

Visioni, D., MacMartin, D. G., Kravitz, B., Richter, J. H., Tilmes, S., & Mills, M. J. (2020). Seasonally modulated stratospheric aerosol geoengineering alters the climate outcomes. *Geophysical Research Letters*, *n/a*(n/a), e2020GL088337. Retrieved from https://agupubs.onlinelibrary.wiley.com/doi/abs/10.1029/2020GL088337 (e2020GL088337 2020GL088337) doi: 10.1029/2020GL088337

Warszawski, L., Kriegler, E., Lenton, T. M., Gaffney, O., Jacob, D., Klingenfeld, D., ... Rockström, J. (2021, May). All options, not silver bullets, needed to limit global warming to 1.5 °C: a scenario appraisal. *Environmental Research Letters*, *16*(6), 064037. Retrieved from https://dx.doi.org/10.1088/1748-9326/abfeec (Publisher: IOP Publishing) doi: 10.1088/1748-9326/abfeec

Zhang, Y., MacMartin, D. G., Visioni, D., Bednarz, E., & Kravitz, B. (2023). Introducing a Comprehensive Set of Stratospheric Aerosol Injection Strategies. *EGUsphere*, *2023*, 1–32. Retrieved from https://egusphere.copernicus.org/preprints/2023/egusphere-2023-117/ doi: 10.5194/egusphere-2023-117

The choice of baseline period influences the assessments of the outcomes of Stratospheric Aerosol Injection

D. Visioni[1,2], E. M. Bednarz[3,4,5], D. G. MacMartin[5], B. Kravitz[6,7] and P. B. Goddard[6]

[1]Department of Earth and Atmospheric Sciences, Cornell University, Ithaca, NY, USA
[2]Atmospheric Chemistry Observations & Modeling, National Center for Atmospheric Research, Boulder, CO, USA
[3]Cooperative Institute for Research in Environmental Sciences (CIRES), University of Colorado Boulder, Boulder, CO, USA
[4]NOAA Chemical Sciences Laboratory (NOAA CSL), Boulder, CO, USA
[5]Sibley School of Mechanical and Aerospace Engineering, Cornell University, Ithaca, NY, USA
[6]Department of Earth and Atmospheric Sciences, Indiana University, Bloomington, IN, USA
[7]Atmospheric Sciences and Global Change Division, Pacific Northwest National Laboratory, Richland, WA, USA

Key Points:

- We analyze results from a set of simulations considering various amounts of cooling using stratospheric aerosols.
- Many of the climatic responses at the surface can be considered linearly related to the amount of cooling.
- The choice of the specific baseline period influences these conclusions.

Corresponding author: Daniele Visioni, `dv224@cornell.edu`

Abstract

The specifics of the simulated injection choices in the case of Stratospheric Aerosol Injections (SAI) are part of the crucial context necessary for meaningfully discussing the impacts that a deployment of SAI would have on the planet. One of the main choices is the desired amount of cooling that the injections are aiming to achieve. Previous SAI simulations have usually either simulated a fixed amount of injection, resulting in a fixed amount of warming being offset, or have specified one target temperature, so that the amount of cooling is only dependent on the underlying trajectory of greenhouse gases.

Here, we use three sets of SAI simulations achieving different amounts of global mean surface cooling while following a middle-of-the-road greenhouse gas emission trajectory: one SAI scenario maintains temperatures at 1.5ºC above preindustrial levels (PI), and two other scenarios which achieve additional cooling to 1.0ºC and 0.5ºC above PI.

We demonstrate that various surface impacts scale proportionally with respect to the amount of cooling, such as global mean precipitation changes, changes to the Atlantic Meridional Overturning Circulation (AMOC) and to the Walker Cell. We also highlight the importance of the choice of the baseline period when comparing the SAI responses to one another and to the greenhouse gas emission pathway.

This analysis leads to policy-relevant discussions around the concept of a reference period altogether, and to what constitutes a relevant, or significant, change produced by SAI.

Plain Language Summary

By adding CO_2 to the atmosphere, the planet warms. As the primary energy input to the system is the Sun, you can try to balance this warming by slightly reducing the incoming sunlight, for example by adding tiny reflecting particles to the atmosphere (aerosols). This cooling will not perfectly cancel the warming from CO_2 due to different physical mechanisms. Understanding how the resulting climate from both effects changes requires a comparison with a "base" state: but there isn't one single choice, something which is made even more clear once one considers multiple amounts of cooling one could do. There isn't only one option as one could decide to just prevent future warming (or some of it), or also try to cancel warming that already happened. Here we explore how the projected outcomes can depend on the base state one selects and which change are linear with the amount of cooling achieved.

1 Introduction

The adverse global impacts produced by human-induced surface warming are well-documented in over 30 years of previous scientific literature and international proceedings. In 1990, the first Intergovernmental Panel on Climate Change (IPCC) Assessment Report already highlighted many of the future challenges and laid the ground for the creation of the United Nations Framework Convention on Climate Change (UNFCCC). The second Assessment Report, in 1995, was essential in informing policy makers on their way to approve the Kyoto Protocols in 1997, where the first legally binding commitment to reduce emissions (by 5% compared to 1990 levels) was ratified. By the time of the Fourth and Fifth assessment reports, observations of rising greenhouse gas (GHG) emissions and concentrations and increasing surface temperatures led the scientific community and the parties of the UNFCCC to determine new emission commitments. These commitments were not just based on emission targets, but also on global mean temperature "thresholds" that the world should commit to not trespassing during this century in order to avoid the worst effects of climate change (Gao et al., 2017). The Paris Agreement clearly stated that the parties were bound (Rajamani & Werksman, 2018) to limit global warming to well below 2, and pursue efforts to limit temperature increase to 1.5 ^{o}C, compared to pre-industrial levels. The need for such thresholds was highlighted in the IPCC Special Report on Global Warming of 1.5°C (Masson-Delmotte et al., 2018), where the risks of staying below 1.5^{o}C as compared to 2^{o}C was discussed in depth.

More recently, multiple studies have shown how countries' commitments and actions are faring against these temperature targets determined in the Paris Agreement, with the general agreement being that almost none of the signatories are actually close to achieving the emission cuts necessary in the short term to remain below 1.5^{o}C (e.g., Kriegler et al. (2018); Brecha et al. (2022)). The current IPCC emission scenarios that maintain temperatures below this threshold (with or without a temporary overshoot) make use of large assumptions of the scalability and deployability of carbon dioxide removal (CDR) technologies in the future (Haszeldine et al., 2018), which some have criticized as unrealistic (Holz et al., 2018; Boettcher et al., 2021; Warszawski et al., 2021). This non-exhaustive and brief description of the last decades of climate change serves here to highlight a conundrum: the risks of surface temperatures going above 1.5^{o}C above preindustrial get clearer with every passing year, and that temperature threshold risks being reached in the next two decades, yet, actual emission cut pledges by all nations that would serve to curtail that warming are not matching what is in international agreement, and the need for a rapid ramping up of CDR necessary to avoid an overshoot (Kriegler et al., 2018) is not matched by current developments in that area.

A potential additional element of a policy response in the short term, allowing for temperatures (and risks) to be managed while emissions are reduced was already discussed by (Crutzen, 2006) with the proposal to reduce a portion of the incoming sunlight by means of injecting sulfate aerosol precursors into the lower stratosphere (Stratospheric Aerosol Injections, SAI hereafter), in order to produce an optically active cloud of aerosol particles with a long lifetime. Crutzen already highlighted risks as well: not only those in the physical realm (changes in stratospheric composition, differences in the forcing of GHG and of the produced aerosols resulting in a climate different from that produced by a reduction of GHG concentrations) but also those in the human and policy realm, namely that the idea itself of SAI could interfere with emission abatements because of the perception that an "easier" option is available. Research in the last two decades has tried to better understand both of those kinds of risks. In the physical sphere, this has been done mainly by simulating the potential effects of simplified SAI deployment scenarios in global climate models, either by injecting some quantity of SO_2 or of other aerosols in the tropical lower stratosphere (Robock et al., 2008; Kravitz et al., 2015), or by simply reducing the solar constant at the top of the model as a proxy (Niemeier et al., 2013; P. Irvine et al., 2019; Visioni, MacMartin, Kravitz, Boucher, et al., 2021; Visioni, MacMartin, & Kravitz, 2021).

In order to understand the impacts of global warming – which ultimately depend on how much greenhouse gas is emitted – the IPCC usually evaluates multiple future scenarios. As the effects of SAI similarly depend on how it is done (e.g., Kravitz et al. (2019)), one cannot make conclusions about the impacts of SAI by only analyzing one scenario. In terms of the magnitude of cooling to achieve, different areas of the world might desire different amounts, and that simply slowing down the warming (MacMartin et al., 2018; P. Irvine et al., 2019), or keeping it at the Paris Agreement threshold of 1.5^{o}C above preindustrial might not be enough for them to stave off the worst or most long term impacts from climate change such as sea level rise (P. J. Irvine et al., 2012). Trade offs between larger coolings and larger impacts from stronger interventions need to be better determined: in (MacMartin et al., 2022) we explained the rationale behind our new sets of simulations which will be used in this work, in which we compare a scenario where, under SSP2-4.5 emissions, SAI is used to keep temperatures at 1.5^{o}C above preindustrial with two other scenarios that further cool by 0.5^{o}C and 1.0^{o}C below that level.

Here we further explore our set of scenarios, leveraging the combination of different comparison periods and of scenarios with different cooling amounts to discuss both the linearity of the surface climate response and to highlight how important the choice of a reference period is when discussing the potential outcomes of SAI. In the following section we will briefly describe the climate model used for this study and then explain more in depth the functioning of the feedback algorithm that determines how to inject SO_2 to achieve the temperature targets in the three SAI scenarios (Section 2). We will then discuss the outcomes in terms of sulfate burden (Section 3.1), surface temperature (Section 3.2) with a focus on the tropical Eastern Pacific response (Section 3.2.1), Atlantic Meridional Overturning Circulation (Section 3.3) and global and regional precipitation (Section 3.4; these all provide examples where the choice of reference period influences interpretations.

2 Methods

2.1 Climate model

In this study we use the Community Earth System Model Version 2 (CESM, Danabasoglu et al. (2020)) in its Whole Atmosphere Community Climate Model Version 6 (WACCM6) configuration with simplified tropospheric chemistry (Davis et al., 2022), hereafter CESM2-WACCM6. This model version has a horizontal resolution of 1.25º longitude by 0.9º latitude with 70 vertical levels that extend up to about 140km. The version we use has comprehensive stratospheric and upper-atmospheric chemistry, as well as an interactive aerosol microphysics scheme termed the Modal Aerosol Module (MAM4) (Liu et al., 2016), but has simplified tropospheric chemistry that only includes the most relevant processes and does not have detailed Secondary Organic Aerosol (SOA) chemistry; in (Davis et al., 2022), this has been shown to not produce relevant changes in stratospheric chemistry and surface climate.

2.2 Simulations design

We consider here three SAI scenarios spanning the period 2035 to 2070, each of which injects the appropriate (more details provided shortly) SO_2 magnitudes required to keep global mean surface temperatures at 1.5ºC, 1.0ºC or 0.5ºC above the preindustrial levels (PI, with the 2020-2039 mean of the CESM model surface temperature data defined as corresponding to the 1.5ºC above PI), respectively (henceforth referred to as SAI-1.5, SAI-1.0, SAI-0.5); motivation and description is given in MacMartin et al 2022. In all cases, GHG emissions follow the Shared Socioeconomic Pathway (SSP) 2-4.5 (Meinshausen et al., 2020).

The SO_2 is injected at every time step, every day of the year at 4 off-equatorial locations - 30ºN, 15ºN, 15ºS and 30ºS, and the yearly injection rates are determined independently at the beginning of each year using a feedback algorithm as in Kravitz et al. (2017). The algorithm computes the injection rates by comparing the annual mean near-surface air temperatures simulated over the previous year to determine how much those values differ from the desired target. This is done not just for global mean near-surface temperature (T0) but also the difference in temperatures between the two hemispheres, computed using the projection of the zonal mean surface temperature onto the first Legendre polynomial (eq. here), and the difference in temperatures between the poles and the equator, computed using the projection onto the second Legendre polynomial ($\ell_0 = 1$, $\ell_1 = \sin(\psi)$, and $\ell_2 = 3(\sin^2(\psi) - 1)/2$, where ψ is the latitude). The target values can be tied to periods in the baseline simulations when T0 had the same 20-year average value: so for SAI-1.5, the period over which T0 is 1.5ºC above PI is 2020-2039 (by definition of our simulations). For SAI-1.0 and SAI-0.5, these periods are 2008-2027 and 1993-2012, respectively, which corresponds to T0 values that are 0.5ºC and 1.0º lower than for the SAI-1.5. Determining this time-period of reference is necessary to calculate the target values for T1 and T2: for all scenarios, these two targets are the values averaged over the reference period.

The controller algorithm uses these targets to determine the needed yearly injection rates of SO_2 at the four latitudes, by estimating the needed projections of the zonal mean stratospheric aerosol optical depth (sAOD) onto the same Legendre polynomials to achieve them and then estimating the injections rates necessary to achieve those sAOD patterns. Information on how the injection of a certain amount of SO_2 translated to a certain shape of sAOD and to a certain temperature response are derived from single-point sensitivity simulations that have been described in Visioni et al. (2023), where all information is available to reproduce the calculations with similar sensitivity simulations in other climate models. The presence of the feedback algorithm is not trying to represent how operationally SAI would work in the real world but should be viewed instead as a modeling tool to allow us to "learn" the set of injection rates needed to achieve a given set of targets.

In all cases, we analyze the responses over the last 20 years of the SAI simulations (i.e. 2050-2069), and compare them against each of the respective baseline periods with the same global mean surface temperature, as well as against the same quasi-present day period, here chosen as the mean over 2020-2039.

2.3 Simulated injection rates

In Figure 1 we show the connection between the imposed SO_2 injection rates and the resulting sAOD patterns and the magnitudes of the global mean cooling. In the top part, we show the total injection rates in the three sets of simulations. In the case of the SAI-1.5 simulation the target (1.5ºC above PI) is reached just a few years before the start of SAI in 2035; therefore the injection rate can be allowed to slowly build up to offset the corresponding global warming (Fig. 1a). In contrast, for SAI-1.0 and SAI-0.5 a "ramp-up" time of 10 years has been built in in the controller to gradually achieve the desired temperature target (and so to avoid a steep temperature change over a few years). After that, changes in injection rates are similar to SAI-1.5, i.e. to just offset the warming from GHGs in SSP2-4.5.

While global mean temperature changes can be tied to the overall injection rates, the management of the other two targets (T1 and T2) depend on the distribution of injection rates over the four locations. Figure 1b shows this distribution as a fraction of the overall injection rates (thereby accounting for the differences in total magnitudes). The distribution of the injection rate during the second part of the simulation (after the initial 10 years) depends on the ratio dT1/dT0 and dT2/dT0 (calculated as the value of T in the reference period minus that in the 2050-2069 period and shown in Table S1), which in turns affect the L1/L0 and L2/L0 ratio needed, which influences the amounts at the various injection locations (MacMartin et al., 2017). In all three cases over half of the injection is determined to be at 15ºS and 15ºN, and the remnant at 30ºS, with no injection at 30ºN. The distribution of injection rates at the onset of SAI is not necessarily consistent in the first 10 years, i.e before the controller converges, as the initial period is influenced by the convergence time of the algorithm and by the initial best guess (based on the sensitivity to the fixed injection rates shown in Visioni et al. (2023)). The hemispheric asymmetry in injection rates is discussed (for simulations in slightly different model configuration) in (Fasullo & Richter, 2023).

In panels 1c-e), we show the projections of the achieved sAOD patterns on the first three Legendre polynomials (termed L0, L1, L2), which relate to the overall magnitude of injection (panel 1a) for L0 and to the locations of the injections for L1 and L2, which indicate how much difference there is in sAOD between the hemispheres (L1) and between tropical and high latitudes (L2) (Ban-Weiss & Caldeira, 2010). In Fig. S1, we also show the relationship between the actual sAOD and the internal control variables indicating the expected values by the controller based on the response in the fixed injection. If the relationship between injection rates and L0, L1, L2 remained linear, then the expected L0, L1, L2 would match the actual. Fig. S1 shows that while the match is very good for SAI-1.5, for higher temperature targets the controller assumes that less SO_2 is

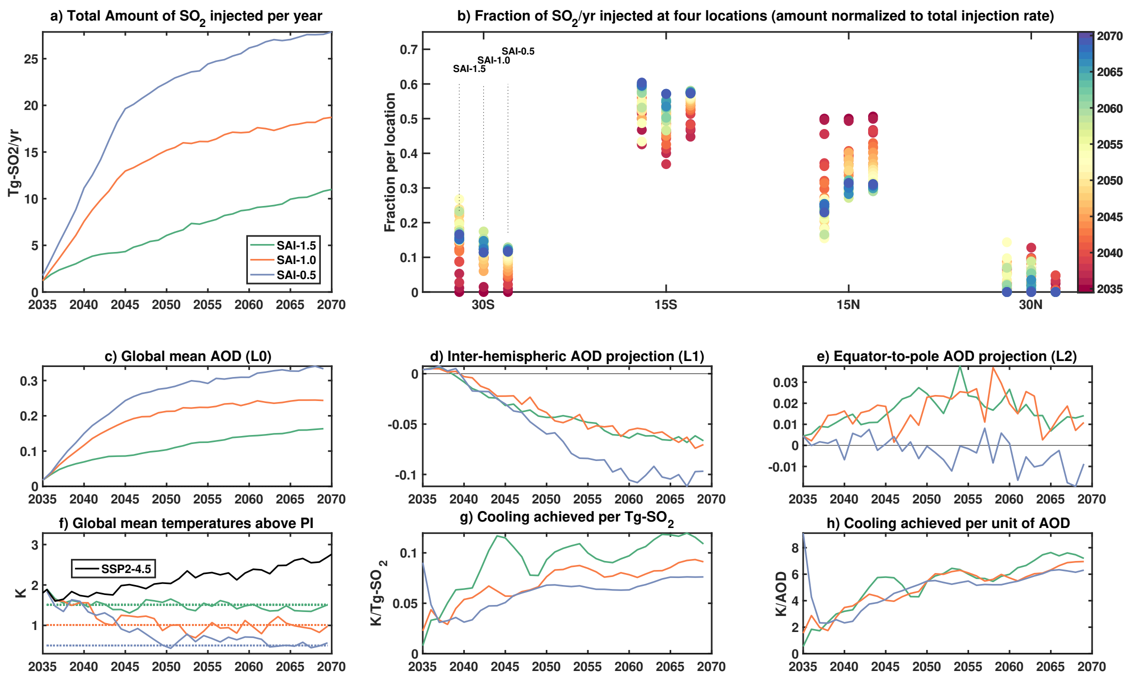

Figure 1. a) Total injection rates in the three sets of SAI simulations. b) Distribution of the injection rates at the four injection locations (30ºS, 15ºS, 15ºN, 30ºN), shown as the fraction of the total amount, color-coded depending on the year from red (2035) to blue (2070); SAI-1.5 is always the leftmost set, followed by SAI-1.0 and SAI-0.5. c-e) Values of L0 (global mean sAOD), L1 (inter-hemispheric sAOD projection) and L2 (equator-to-pole sAOD projection). f) Global cooling achieved in the SAI simulations compared to preindustrial (PI) temperatures. g) Efficacy of cooling per 1 Tg of SO_2 injected. h) Efficacy of cooling per sAOD produced. A 5-years running mean is applied to panels g) and h). For clarity, only the ensemble averages are shown in all panels.

needed to achieve a certain sAOD pattern. This points to nonlinearities in the injection rate to AOD conversion under high injection rates, which could arise from larger effective radii and shorter aerosol lifetime (particularly for L0) and from dynamical changes in the stratospheric transport (for L1 and L2) due to stronger lower stratospheric warming in the tropics (Visioni, MacMartin, Kravitz, Lee, et al., 2020). The differences in L1 for SAI-0.5 are driven by a value of dT1/dT0 (Table S1) that is 28% larger compared to that in SAI-1.5; similarly, the L2 differences are driven by a dT2/dT0 value that is 25% smaller in SAI-0.5 compared to SAI-1.5.

Figure 1f shows the simulated global mean temperatures above PI conditions and, thus, illustrates the overall cooling achieved in the three simulations compared to the warming in the SSP2-4.5 scenario (also shown in MacMartin et al. (2022)). Over the last 20 years of the three SAI simulations, the difference in global mean temperatures compared to the same period in SSP2-4.5 is 0.9 ºC (SAI-1.5), 1.4 ºC (SAI-1.0) and 1.8 ºC (SAI-0.5). Finally, in panels g) and h) we show how this cooling relates to the injected amount of SO_2 and to the unit of global mean AOD. We find that the relationship between the total SO_2 injection and the resulting global mean cooling is sublinear (i.e. the strongest efficacy is found for SAI-1.5); similarly, a lower cooling per unit AOD is achieved, with a value of 6.5, 6.1 and 5.7 K/AOD for SAI-1.5, SAI-1.0 and SAI-0.5 respectively. Both sublinearities are due to microphysical nonlinearities (Niemeier & Timmreck, 2015; Visioni, MacMartin, Kravitz, Lee, et al., 2020) as larger aerosols have lower lifetime as they're heavier and they are also less efficient scatterer (Laakso et al., 2022). Hence, while 10 Tg-SO_2 are necessary in SAI-1.5 to cool by 1ºC, the next 10 Tg-SO_2 only cool by 0.7ºC in SAI-0.5, thereby requiring 26 Tg-SO_2 to cool to the desired target of 1.8 ºC, instead of 18 Tg-SO_2 if the relationship had remained the same as in SAI-1.5.

3 Results

3.1 Sulfate burden

In Figure 2 we show the changes in the stratospheric sulfate burden produced by the injections described in Section 2.3. A comparison of panels a-c) highlights the large differences in the sulfate concentrations between the three SAI strategies, in line with the differences in cooling and injection rates reported in Fig. 1. SAI-1.5 increases the sulfate burden by up to 40 μg-S/kg-air in the tropical lower stratosphere (as compared to 1 μg-S/kg-air in the unperturbed stratosphere, while SAI-0.5 peaks at 108 μg-S/kg-air). Similarly, the overall increase in column burden as shown in panel 2d is 20.2 mg-S/m2 for SAI-1.5 and 52.6 mg-S/m2 for SAI-0.5. Despite large differences in total sulfate burden, all 3 SAI simulations show similar horizontal distributions with the largest sulfate burden (Fig. 2d) and sAOD (Fig. 2e) increases in the Southern Hemisphere, consistent with the similarities in the distributions of the injection rates in Fig. 1b. The significantly larger (by a factor of $\sim$2) amount of aerosols in the Southern Hemisphere than the Northern Hemisphere is necessary in this model version in order to manage the inter-hemispheric temperature gradient (see Fasullo and Richter (2023) for details and for a discussion of differences with CESM1).

Fig. 2f and 2g, together with Fig. 1g and 1h further inform whether the achieved cooling is linear with respect to increasing injection rates. Fig. 2g indicates that in the three scenarios the injection rates and produced AOD are proportional, but the coefficient of the linear fit between the three is different because of dynamics in the first part (higher injections in the first years mean that AOD needs some years before it converges) and because of microphysical nonlinearities in the second. Therefore, if one only had the SAI-1.5 simulation, and assumed linearity and excluded the first 10 years as SO_2 to AOD converges, they would conclude that it would take 24 Tg-SO_2 to achieve a global AOD of 0.3, whereas in SAI-0.5 it takes 26, an 8% error. Similarly, Fig. 1h and Fig. 2g show that the same unit of AOD results in a slightly different amount of cooling: 6 K per unit of AOD globally, in SAI-1.5, and 7 in SAI–0.5), a 14% difference. Overall, both sub-linearities

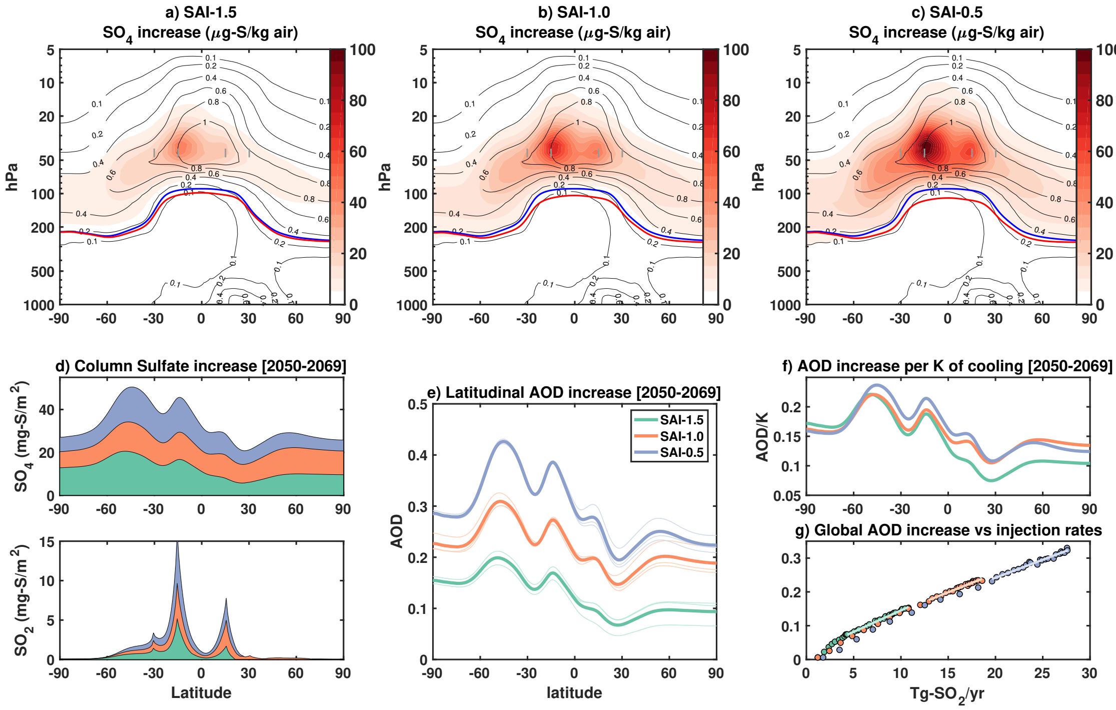

Figure 2. a-c) Shading: Zonal mean increase in sulfate mass concentrations (in ug-S/kg-air) for the 2050-2069 period in the three SAI experiments (SAI-1.5, SAI-1.0 and SAI-0.5 compared to the 2020-2039 period in the background SSP2 simulation (shown as thin contour lines). Blue line indicates the average annual tropopause height in the background SSP2 simulation for the 2020-2039 period, red lines indicate the same quantity for the three respective SAI simulations over 2050-2069. d) Zonal mean increase in the overall column burden in the three simulations for SO4 (top) and SO_2 (bottom) for 2050-2069. e) Zonal mean stratospheric optical depth (sOD) increase for 2050-2069, lighter lines show single ensemble realizations. f) Zonal mean increase in stratospheric optical depth (sAOD) normalized by the resulting cooling over the same period. g) global mean AOD as a function of SO_2 injected in the same year.

compound in those found in Fig. 1g and discussed in Section 2.3, resulting in a 31% error in estimating the required injection to achieve the cooling in SAI-0.5 based on the SAI-1.5 simulations.

3.2 Temperature response

An important question when discussing the possible surface response to SAI is "What should simulations of SAI be compared against?". We offer as an example one previous comparison available in the literature: the GeoMIP G6sulfur simulation protocol (Kravitz et al., 2015). This simulation protocol used a scenario following the SSP5-8.5 emissions and prescribed an intervention where SAI was applied to bring temperatures down to those in a scenario following theSSP2-4.5 emissions. For a future period simulated with SAI, one could thus compare a certain quantity (mean temperature, mean precipitation, frequency or intensity of a type of extreme event) against both SSP5-8.5 and SSP2-4.5 and observe which spatial differences are present in G6sulfur minus SSP2-4.5, and contrast them with those between SSP5-8.5 and SSP2-4.5.

In our case, our set of simulations can help us expand this comparison by being more explicit on what our goals are. The central problem with GHG-induced global warming (as a measure of other changes) is that it shifts the climatic state outside of historical climate variability, it does so too fast for ecosystems and human adaptation capabilities, and it risks approaching irreversible changes in the system (i.e. tipping points, Lenton et al. (2008)). The comparison of a future (SSP2-4.5) and past period helps identify these changes, with different future GHG concentration levels dictating the amount of warming (Meinshausen et al. (2020), not shown here). SAI introduces a new dimension, as the stratospheric aerosol cooling, on top of increasing GHG concentrations, can reduce the increase of global mean temperatures, stop it, or even cool down to a previous level compared to present days. Evaluations of the SAI+GHG scenarios can thus compare them against:

1. Future periods without SAI, but with the same GHG concentrations (and higher global temperatures), which which is relevant for comparative impact assessment.
2. Present day period, hence with lower GHG concentrations, which highlights differences with currently experienced climate by highlighting "deviations" from a (somewhat arbitrarily chosen) baseline state, though deviations from this state do not directly convey information about impacts.
3. Periods with same global mean temperature, but lower GHG concentrations (with the same caveats). Depending on the SAI scenarios, some of these periods might overlap or hold different meanings: in the G6sulfur example, (3) also indicates a future period, but with less warming because of the underlying SSP scenario, and "present day" is cooler than both.

In the cases under analyses here, SAI-1.5 cools by construction exactly at the "present day" level (2020-2039), while SAI-1.0 and SAI-0.5 cool further, allowing for a three point comparison between SSP2-4.5, SAI and baseline cases. Finally, instead of selecting just one "baseline" with a strict comparison of periods with the same global mean temperature, one can compare against a larger portion of the historical period, focusing on understanding when the compensation of GHG warming with SAI cooling results in a state that lies in a certain range of historical variability.

Examples of comparisons as outlined above are given in Figure 3 for the spatial distribution of temperature changes in the last 20 years of simulation. Top row panels show the regional effects of global temperature warming under SSP2-4.5 by comparing the future period with present or past periods with lower global mean temperature. Comparing SSP2-4.5 with 'present day' (2020-2039, BASE-1.5) already shows changes detectable everywhere on the globe, with a global average increase of 1.3 ºC. By comparing the same time period in the SAI-1.5 simulation against this reference, we can observe how "effective" our simulated SAI strategy is in offsetting the GHG-induced warming. Using a double-sided t-test to determine statistical significance at a 95% level, temperature changes would be detectable only in 27% of the world compared to BASE-1.5. As the 1.5 ºC threshold is, in many ways, arbitrary, one can also choose to compare against other periods, such as when temperatures were cooler, e.g. the 2008-2027 (BASE-1.0) and 1993-2012 (BASE-0.5). If SAI only cools globally by 0.8 ºC (as in the SAI-1.5 simulation), then most areas will still be warmer than 0.5ºC above PI. A similar statement can be made for the other simulations and other possible reference periods. In Fig. 3 we highlight this aspect by representing the overall space of possible comparisons using a matrix approach in which rows represent any future simulation (either SSP2-4.5, SAI-1.5, SAI-1.0 or SAI-0.5) and the columns represent a potential target to compare our future simulation against.

The diagonal panels in Fig. 3 show changes in SAI-1.5, SAI-1.0 and SAI-0.5 against their target periods, BASE-1.5, BASE-1.0 and BASE-0.5 (i.e. the periods in the past with the same 20-year-mean global mean temperature). This comparison highlights that more cooling results in more areas that show statistically significant temperature changes. Among these changes is a temperature increase over the Eastern Pacific, projecting onto the pattern associated with the positive phase of the El-Nino Southern Oscillation (ENSO), and a temperature decrease over the Northern Atlantic, indicating a weakening of the At-

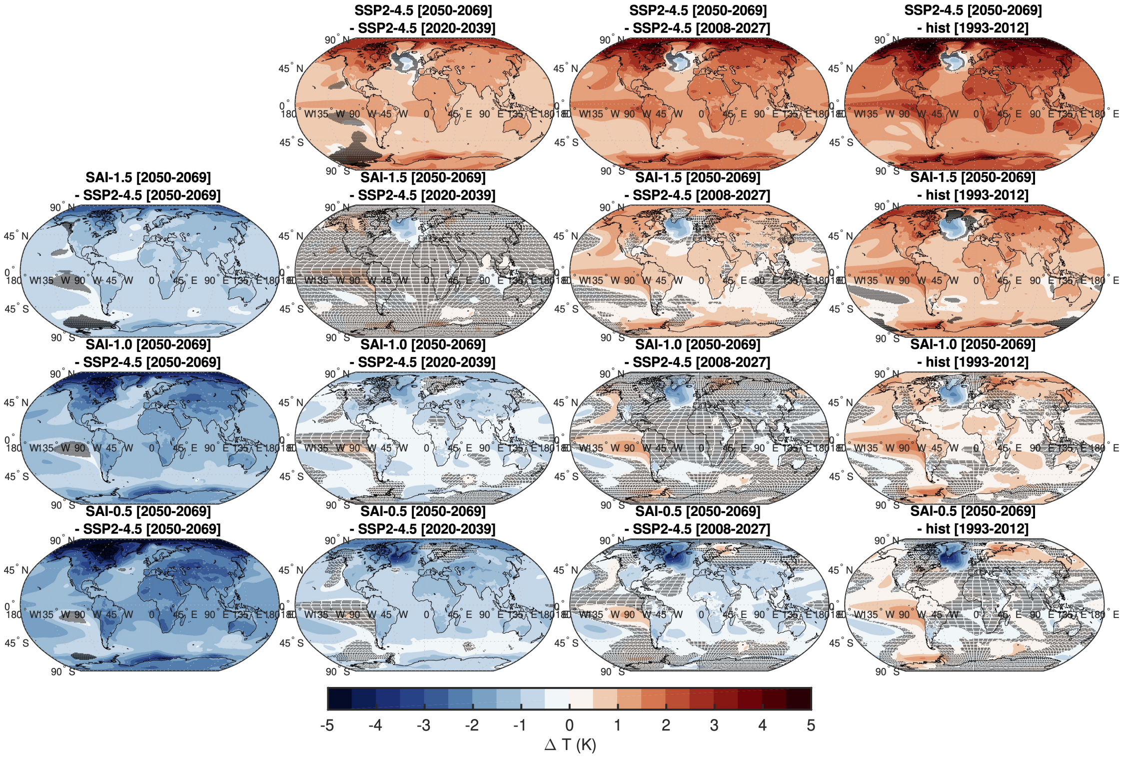

Figure 3. Comparison of surface temperatures changes averaged over 20 years periods and all ensemble members. The rows indicate the first term of the comparison, while the columns indicate the second. SSP2-4.5 [2050-2069] is both the first row and first column, indicating the reference future with an increase in CO_2 concentrations that is unabated by SAI. The other three rows show the three SAI simulations, from the one cooling the least (SAI-1.5) to the one cooling the most (SAI-0.5). The other three columns indicate the reference period selected, from the future to the historical period [1993-2012] (as simulated in CESM2-WACCM6).

lantic Meridional Overturning Circulation (AMOC). Both of these responses are analyzed in more depth in Sections 3.2.1 and 3.3. Items of comparison outside of the diagonal in Fig. 3 also offer valuable information. For instance, the comparison between SAI-1.5 and SSP2-4.5 (second row, third column) shows the results in which warming between SSP2-4.5 in 2050-2069 and BASE-1.0 (which equates to a 1.5^{o}C temperature difference) is halved rather than considering it as an SAI case in which the whole warming from the period 2020-2039 is offset. In this case, one could argue that the cooling produced is moderate (P. Irvine et al., 2019; P. J. Irvine & Keith, 2020) (i.e. it doesn't offset the whole amount of warming) and thus would incur less SAI-induced changes (albeit most areas in such a strategy, by definition, would still be warmer than the period under comparison).

In general, we highlight that the particular choice of a baseline period can yield different results, speficically in the perceptual sense of discussing if a particular feature looks "better" or "worse" under SAI, and while having a context in which to understand mechanistic changes to climatic features is important (as we will discuss in the following sections), it might always result in biased assessments of the role of SAI (Reynolds, 2022). It is crucial therefore to think of better ways to interpret changes due to SAI to make sure future assessments are more meaningful.

3.2.1 Eastern tropical Pacific response

El Niño/Southern Oscillation (ENSO) is one of the main climatic modes of variability, the teleconnections of which have worldwide impacts (Timmermann et al., 2018). During El Niño periods an anomalous sea surface temperature (SST) warming pattern can be identified in the eastern/central Pacific, replaced by an anomalous SST cooling pattern during La Niña. These anomalies in the Pacific sea-surface temperatures are strongly coupled to changes in atmospheric convection and Walker Circulation, thereby affecting weather patterns on both sides of the Pacific Ocean. ENSO is a complex and highly variable phenomenon, and understanding its changes and impacts requires a detailed representation of a complex interplay of ocean and atmospheric processes.

Under GHG-induced warming, an increased equatorial Pacific warming and a weakening of the Walker circulation (Vecchi et al., 2006) are projected to lead to a stronger ENSO magnitude and frequency (Cai et al., 2015); this has been inferred through ENSO proxies (Grothe et al., 2020), reanalyses and multi-model projections (Cai et al., 2021). Given the need for long simulations in order to properly sample the underlying processes, provided the high variability and a comparatively long period of an average ENSO cycle, few results are available for SRM simulations. (Gabriel & Robock, 2015) examined a range of different GeoMIP G1-G4 experiments and found no statistically robust changes in ENSO characteristics under geoengineering compared to those driven by the GHGs alone. (Malik et al., 2020) used a 1000-year-long solar dimming simulation to assess changes in the mean state and extreme ENSO events, and found some significant changes compared to preindustrial. Such changes were, however, in large part driven by the tropical overcooling typical of solar dimming simulations (Visioni, MacMartin, & Kravitz, 2021) and would thus not be representative of more complex SAI strategies maintaining multiple surface temperature gradients such as those analyzed here.

In the absence of SAI, the simulated (20-year mean) SST pattern in the Pacific Ocean is similar to the positive phase of ENSO, (Fig. 3, first row), potentially due to similar mechanisms as the projected intensification of the El- Niño events under GHG-induced warming and the weakening of the Walker Circulation (see Section 3.4.1, Fig. 7) . Despite the cancellation of the global mean surface temperature increase under SAI, when the different SAI scenarios are compared against each individual baseline period the simulations still show increased SST in the eastern Pacific, suggestive also of a mean response with a pattern similar to the positive phase of ENSO that is not compensated by the SAI global cooling, statistically significant for SAI-1.0 and SAI-0.5 (diagonal maps in Fig. 3).

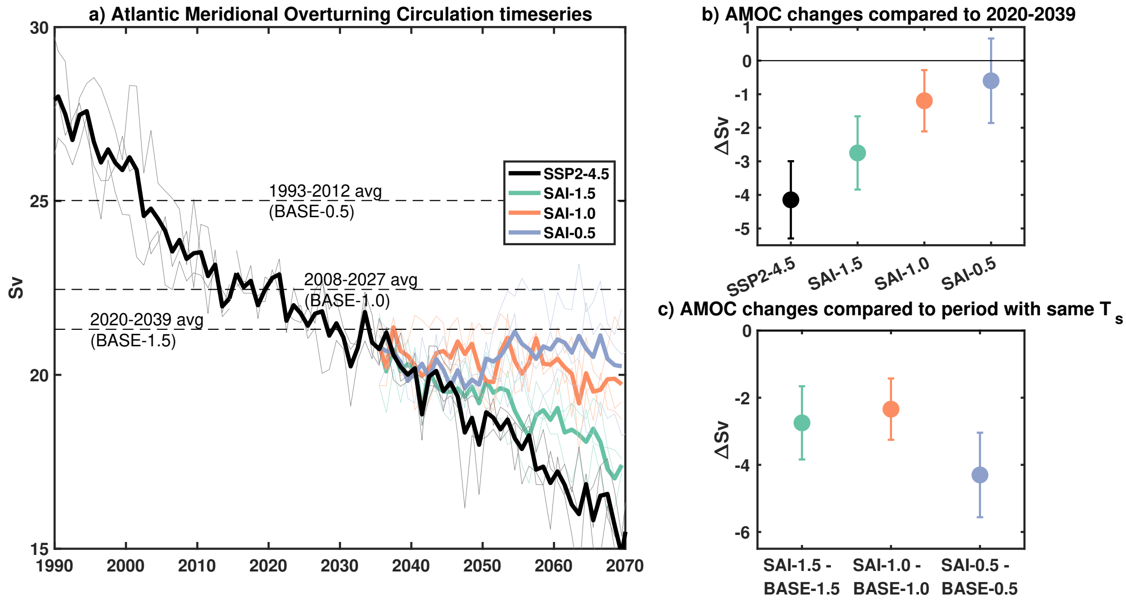

Figure 4. a) Yearly mean values of AMOC strength in all simulations, defined as the maximum value of the North Atlantic meridional overturning streamfunction. Lighter lines indicate single ensemble realizations, while thicker lines indicate the ensemble average. b) Changes in AMOC strength in 2050-2069 compared to the values in the period 2020-2039. The error bars indicate ±1 standard error of the difference in means. c) Changes in AMOC strength in 2050-2069 for the three SAI simulations compared to their respective period with the same global mean surface temperature.

3.3 AMOC response

Fig. 4a shows a timeseries of the simulated AMOC strength, while Fig. 4b shows the associated twenty year average changes in 2050-2069 compared against the same quasi-present day BASE1.5 period and Fig. 4c shows the twenty year changes compared against each individual baseline period. In the absence of SAI, the strength of AMOC decreases under SSP2-4.5 because of the polar amplification and the resulting weakening of the temperature and salinity vertical gradients in the Northern Atlantic (Fasullo et al., 2018; Fasullo & Richter, 2023).

We find that all SAI scenarios slow AMOC weakening, with the effectiveness increasing marginally under increased magnitude of SAI. Importantly, the differences in the AMOC response among the three different SAI scenarios, when compared against the same BASE1.5 baseline period, are much smaller than the long-term GHG-induced AMOC trend under SSP2-4.5 alone when compared against the three different baseline periods. Thus, if one chooses to compare the SAI AMOC responses against their respective baseline periods the results show increased weakening under increased magnitude of SAI. In contrast, comparing the SAI AMOC responses against the same quasi-present day baseline period the results show reduced weakening under increased magnitude of SAI. This inconsistency is primarily driven by the differences in AMOC strength during the different reference periods, i.e. before SAI started. This analysis is another example presented here which highlights the importance of the chosen baseline period when evaluating the SAI responses under different magnitudes of global cooling.

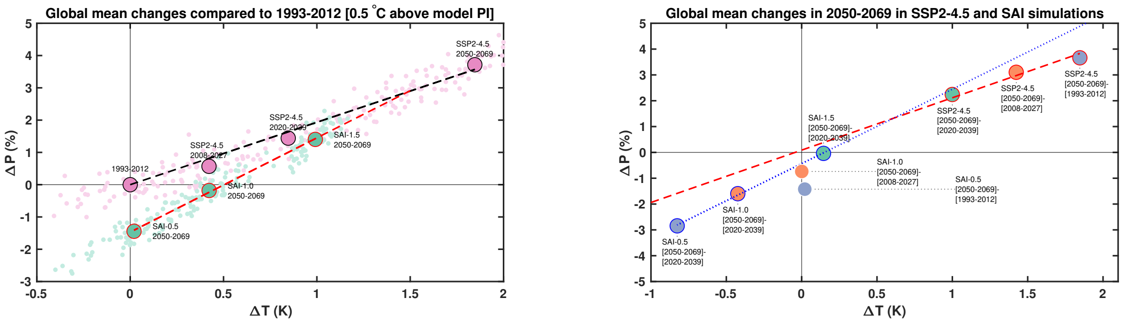

Figure 5. Changes in global mean temperature (K) compared to changes in precipitation (as a percent of the baseline precipitation, %), representing the Hydrological Sensitivity to both GHG-induced warming and SAI-induced cooling. In panel a), the values are represented against the coldest period analyzed in this work (1993-2012, 0.5ºC above PI), for all three warmer periods due to GHG (2008-2027 for 1.0ºC above PI; 2020-2039 for 1.5ºC above PI; and 2050-2060 for 2.4ºC above PI) and for the three SAI simulations in the period 2050-2069 with the three different levels of cooling. The single yearly values for each period and all ensemble members are also shown. In panel b), SAI values in 2050-2069 are compared against the 2020-2039 reference period, while the SSP2-4.5 values in 2050-2069 are compared against time periods which represent cooler temperatures in SSP2-4.5 in increments of0.5ºC.

3.4 Precipitation response

The precipitation response to changes in temperature has been previously investigated both for GHG-induced warming and for simulated SAI cooling . For abrupt 4xCO_2 experiments in the literature, this response can be typically divided into a fast (cloud, vegetation and radiative response to the perturbation) and a slow (usually identified with a temperature-driven response) contribution (Tilmes et al., 2013; Cao et al., 2015).

Under long-term changes in tropospheric temperatures, global mean precipitation tends to scale linearly with the surface temperatures. This relationship (called hydrological sensitivity, HS) can be explained in terms of changes to the energy balance of the atmosphere, and is a combination of the fast and slow response described above (Held & Soden, 2006; Pendergrass & Hartmann, 2014). The linearity of this response has been shown to hold in both modeling studies (Kvalevåg et al., 2013) and observational studies (DelSole et al., 2016), but with spread between individual models (Fläschner et al., 2016) and with considerable uncertainties over the available measurements (DelSole et al., 2016). In general, for the GHG-induced warming, the modeling consensus lies around 2-3% precipitation increase per 1 K of warming (Samset et al., 2018). For CESM, this is confirmed in Fig. 5 where we show a HS of 2.0% increase per K of warming in SSP2-4.5 as compared to the three reference periods with 1.5, 1.0 and 0.5 ºC above the model PI.

For SRM, multiple modeling studies reported that for a certain amount of cooling, global precipitation would be reduced more compared to a GHG-induced increase (Niemeier et al., 2013; Tilmes et al., 2013), leading to what is usually termed as an "overcompensation of precipitation versus temperature". Thermodynamical changes in the vertical temperature gradient is shown to be one of the reasons behind this, as the forcing from elevated CO_2 cannot be perfectly matched by a reduction in the incoming solar radiation, due to different mechanisms as the former warms from the bottom-up, and the latter cools from the top-down (Govindasamy et al., 2003; Ricke et al., 2023). Other reasons include the contribution of the aerosol-induced stratospheric heating under SAI (Simpson

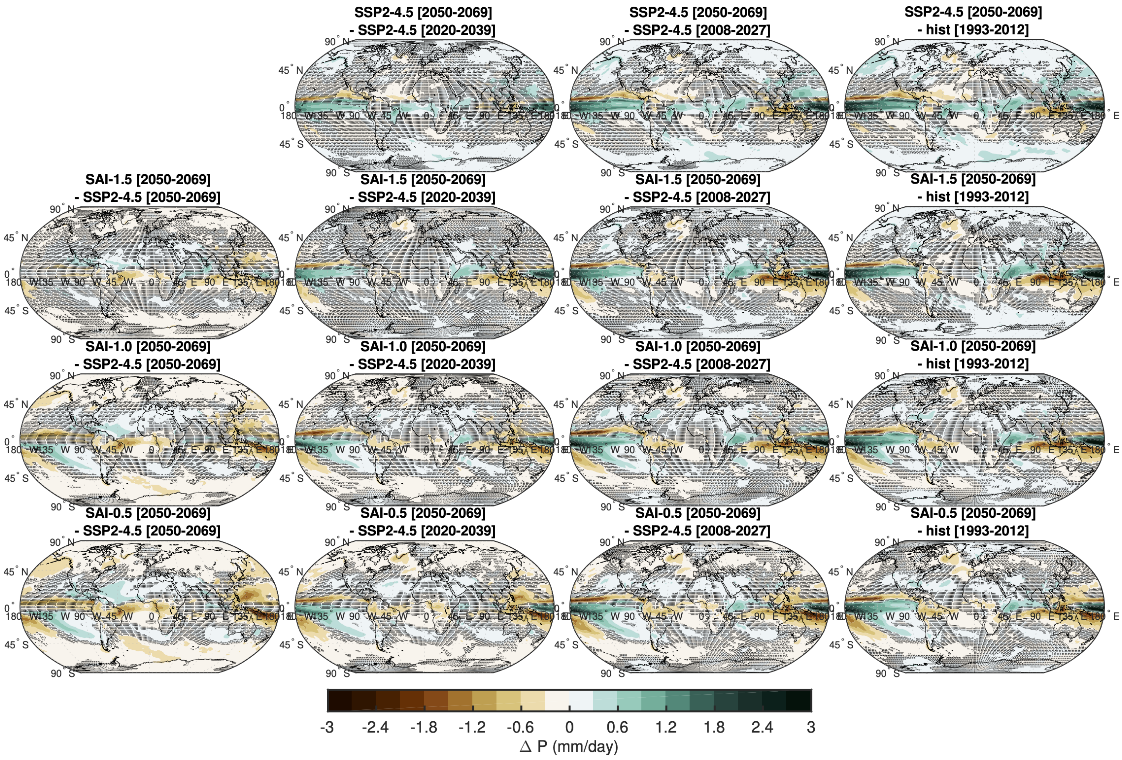

Figure 6. As in Fig. 3, but for the yearly mean precipitation response (mm/day).

et al., 2019; Visioni, MacMartin, & Kravitz, 2021) or differences between the land response to shortwave versus longwave forcing (Niemeier et al., 2013). As shown in Fig. 5, the SRM-specific changes are also confirmed in our simulations with different levels of cooling as the slope of the linear fit for the SAI simulations when compared to the same reference period (2020-2039) is steeper than the warming-derived one (2.9% decrease per K of cooling). Similarly, when the SAI simulations are compared against their respective baseline periods the difference between the two slopes is also evident. In these cases, the data points for SAI-1.0 vs BASE-1.0 and SAI-0.5 vs BASE-0.5 indicate, by definition, no changes in the global mean surface temperature; yet, the corresponding reduction in the global mean precipitation grows larger with increasing levels of SAI. This change in hydrological sensitivity induced by the compensation of GHG-warming with SAI can be estimated to be equivalent to a 0.9% decrease per SAI-induced cooling.

3.4.1 Regional changes

Regionally, precipitation changes will reflect modulations of the large-scale tropospheric circulation patterns. At this spatial scale, these changes are driven by the position and intensity of the Hadley (including the behavior of the Intertropical Convergence Zone, ITCZ) and Walker Circulations as well as monsoonal circulation due to the different temperature response between land (which warms or cools faster) and ocean.

The SSP2-4.5 precipitation response largely reflects the southward shift of the ITCZ (Fig. S2) due to different rates of warming between the hemispheres, potentially also driven by different tropospheric aerosol emissions (cite), alongside the overall increase in the global mean precipitation caused by the increase in the global mean surface temperatures. The combination of these two factors leads to an increase in yearly mean precipitation in equatorial Africa (Fig. 6). In the eastern Indian and western Pacific Ocean regions, the weakening and eastward shift of the Walker Circulation in SSP2-4.5 (Fig. 7)

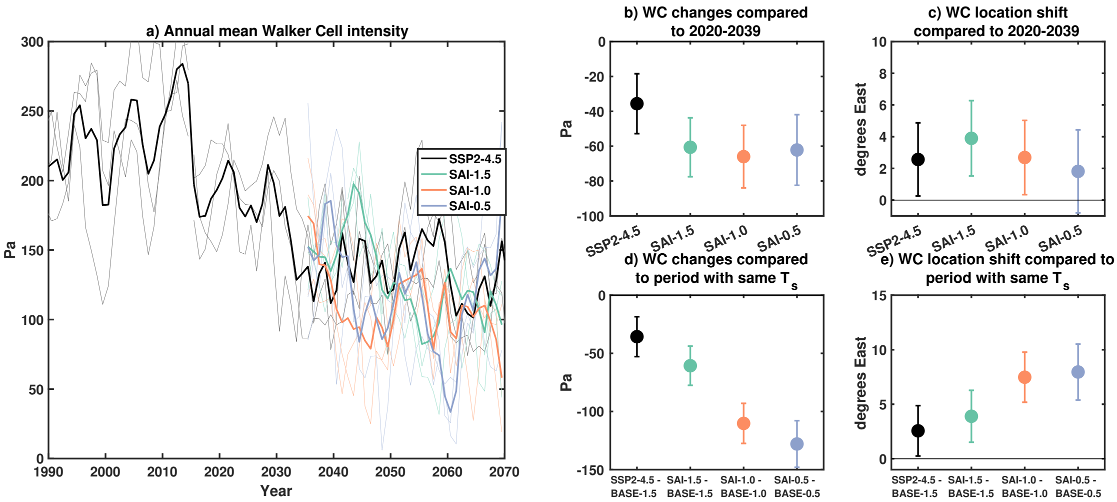

Figure 7. a) Annual mean Walker Circulation (WC) intensity for all experiments, with a 5-year moving average. b) Annual mean changes in the WC intensity from 2050-2069 compared to 2020-2039, and c) annual mean changes in the location of the transition between the anti-clockwise and the clockwise cells over the Indian Ocean and Western Pacific for the same time periods. d) Annual mean changes in the WC intensity for the three SAI simulations compared to each respective time period with the same global mean surface temperature, and e) annual mean changes in the location of the transition between the anticlockwise and the clockwise cells over the Indian Ocean and Western Pacific for the same time periods. The intensity of the Walker circulation is calculated using the SLP-base method (see text for details). The error bars indicate ± 1 standard error of the difference in means.

initiates a reduction in precipitation in the Indonesian region. We use two metrics of the Walker Circulation: i) a pressure based index of its intensity, defined as the difference in sea level pressure between east/central Pacific (160W-80W, 5S-5N) and western Pacific (80-160E, 5S-5N), as in Kang et al. (2020); and ii) the location of the individual cells of the Walker Circulation, estimated from the zonal mass streamfunction. The latter is calculated using the divergent component of zonal wind, averaged over 10S-10N, following the formula in (Guo et al., 2018). The longitudinal shift of the Walker Circulation is approximated by the shift of the zero line in the stream function at 400 hPa over the Indian Ocean and Western Pacific (80E-200E).

The weakening and eastward shift of Walker Circulation has been commonly simulated in climate models as a result of rising greenhouse gas levels and, thus, changes in static stability and lapse rate brought about by upper tropospheric temperature changes (e.g. Bayr et al. (2014); Nowack et al. (2015)). The weakening of the Walker Circulation under global warming is also consistent with the projected intensification of the El-Niño like events discussed in Section 3.2.1.

As discussed in Section 3.4, no significant change to global mean precipitation is simulated in SAI-1.5 (compared to 2020-2039), and the small decreases in SAI-1.0 and SAI-0.5 is due to the associated decreases in the global mean temperatures (Fig. 5). Regarding the ITCZ position, the use of the feedback algorithm controlling the interhemispheric temperature gradient (T1) reduces the magnitude of the ITCZ shift in the SAI simulations compared to SSP2-4.5 (Fig. S2). Yet, a small ITCZ shift is nonetheless found in all SAI simulations illustrating that the feedback control over T1 is not a sufficient constraint. The magnitude of the ITCZ shift is however similar among the three SAI scenarios.

Aside from the thermodynamically-driven changes in global mean precipitation and those arising from shifts in the tropical zonal mean circulation and ITCZ, the SAI simulations also show relevant changes to the tropical Walker Circulation (Fig. 7). In particular, all three SAI simulations show a weakening and an eastward shift of the Walker circulation, the magnitude of which increases with more cooling when the SAI simulations are compared against their respective baseline period. In contrast, when compared to the same quasi-present day baseline period, the SAI simulations show little change to the strength or position of the Walker Circulation under increasing magnitude of SAI. Notably, the sea-level pressure anomalies in the eastern Pacific strengthen under increasing magnitude of SAI forcing but the anomalies in the western Pacific weaken(Fig. S4). This result leads to similar changes of the Walker Circulation intensity across the three SAI scenarios in Fig. 7 and suggests that factors other than global mean temperature contribute to the Walker Circulation and precipitation response in the region under SAI. The contrasting behavior which is dependent upon the baseline period likely reflects the contribution of the GHG-induced changes in the Walker Circulation during the period before SAI is started. These different baseline periods reflect different background (i.e. non-SAI) forcings as shown by the large differences in the SSP2-4.5 responses as compared to its temperature-dependent baseline periods (Fig. 7 and S3). This result highlights the importance of considering the baseline period when interpreting SAI impact on Walker Circulation.

4 Conclusions

In this work, we presented results from multiple sets of Stratospheric Aerosol Injection (SAI) simulations in which SO_2 injections at four different latitudes are used to maintain annual and global mean surface temperatures at 1.5, 1.0 and 0.5 $^{\circ}$C above preindustrial (PI) levels (SAI-1.5, SAI-1.0 and SAI-0.5 respectively) while greenhouse gas emissions follow the CMIP6 SSP2-4.5 scenario.

The analyses serve to better understand the linearity of the climate response to the different magnitudes of SAI. Furthermore, this work can help inform the design of an emulator to be used to analyze comparatively large sets of SAI scenarios that would not be computationally feasible using a fully-coupled Earth system model.

The three SAI scenarios all start SO_2 injections in 2035 and continue through 2069, with analyses focusing on the last 20 years (2050-2069). For each of these SAI scenarios, a corresponding 20-year-long baseline period is established from the SSP2-4.5 and/or historical simulation (without SAI) that has the same global mean temperature: 2020-2039 for SAI-1.5, 2008-2027 for SAI-1.0 and 1993-2012 for SAI-0.5. The choice of this baseline period with the same global mean surface temperature permits an evaluation of the diverse distribution of impacts arising from the imperfect compensation of the GHG-induced warming with the cooling produced by the sulfate. Additionally, comparing the SAI simulations against the same future period from the reference SSP2-4.5 scenario without SAI facilitates an evaluation of the direct effectiveness of SAI compared to a future climate modified by the GHG-induced warming. Finally, a comparison of the SAI scenarios and their impacts against the present day baseline period (here taken as 2020-2039) provides valuable information for future SAI decision making processes. In addition to stressing the importance of the choice of baseline period has for the context of the discussion, we also presented a couple of examples when the choice of baseline period can spuriously affect the conclusions regarding the effectiveness and linearity of the SAI responses (e.g. on the strength of AMOC or Walker Circulation) under varying magnitudes of the global mean surface cooling.

The main goal behind these simulations and of this work is to illustrate that an evaluation of SAI impacts needs to take into account multiple dimensions in order to highlight trade-offs and properly identify the space of possible SAI-driven impacts (MacMartin et al., 2022). Here we have focused on the amount of cooling that SO_2 is chosen to produce, a method that is similar to the scenario exploration under different GHG concen-

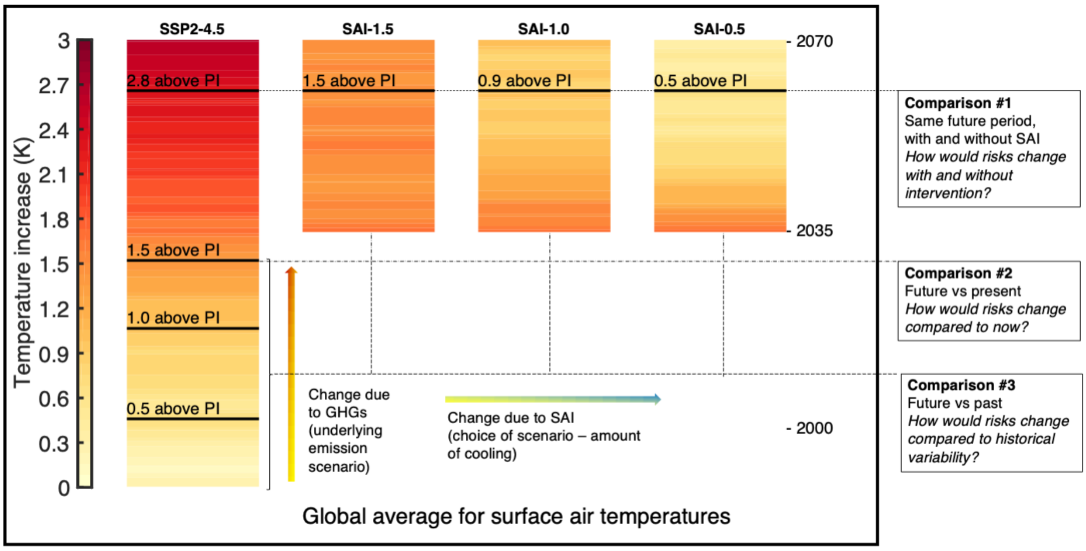

Figure 8. A schematic figure reflecting on the potential choices of comparison periods when discussing SAI impacts. Colorbar indicate global mean, ensemble mean average for surface temperature (K) as a deviation from the PI value.

trations in the IPCC scenarios (Meinshausen et al., 2020). In other works, the way in which some impacts are driven by different SO_2 injection locations (the injection strategy) has been explored (Kravitz et al., 2019; Visioni, MacMartin, Kravitz, Richter, et al., 2020; Bednarz et al., 2023; Zhang et al., 2023). Together these studies provide an overview of the possible design space of SAI that form a foundation for future SAI explorations in a multi-model framework.

This work highlights that SAI studies, by adding a novel dimension to the ability to influence global warming impacts, need even more care when explaining how they are defining a certain simulated impact. Comparisons between different baseline periods can yield different insight onto what constitutes a direct SAI impacts, as opposed to what constitutes an imperfect compensation between GHG-induced warming and SAI: for instance, a change in tropospheric circulation due to stratospheric heating (Simpson et al., 2019; Bednarz et al., 2022) as opposed to the sea-land contrast not restored due to different heat capacities resulting in monsoonal circulation changes (Visioni, MacMartin, Kravitz, Richter, et al., 2020). While such comparisons are fundamental for determining some of the physical drivers (and thereby, might warrant SAI simulations with higher signal-to-noise ratio), it is hard to capture the nuance when discussing potential impacts and risks from a policy-relevant perspective. The choice of reference period is also relevant because people will interpret such comparison plots to infer influences on climate impacts, e.g., noting that some precipitation or temperature feature is over- or under-compensated relative to the compensation of global mean temperature; that SAI creates a "novel" climate state. In this sense, though, any choice of current or historical reference period is potentially misleading: if some climate variable is restored to levels consistent with the past period when global mean temperature was 1.5ºC above preindustrial, and some other variable restored to levels consistent with an earlier historical period when global mean temperature was 1.0ºC, it is entirely unobvious what the influence of that novel climate state would have on human or ecosystem impacts, and the answer would depend on what changes have already been adapted to, for example. For this reason, it is important to stress that there is no single reference period relevant for inferring ultimate impacts and indeed it may be more appropriate to compare to a range of past conditions rather than to any single state (Figure 8).

5 Open Research

All model output analysed in this work is available at https://doi.org/10.7298/xr82-sv86 (Visioni, 2022).

Acknowledgments

We would like to acknowledge high-performance computing support from Cheyenne (https://doi.org/10.5065/D6RX99HX) provided by NCAR's Computational and Information Systems Laboratory, sponsored by the National Science Foundation. Support was provided by the NOAA cooperative agreement NA22OAR4320151, NOAA Earth's Radiative Budget initiative, Cornell Atkinson Center for Sustainability, and by the National Science Foundation through agreement CBET-2038246. Support for BK was provided in part by the National Science Foundation through agreement SES-1754740 and the Indiana University Environmental Resilience Institute. The Pacific Northwest National Laboratory is operated for the US Department of Energy by Battelle Memorial Institute under contract DE-AC05-76RL01830.

References

Ban-Weiss, G. A., & Caldeira, K. (2010). Geoengineering as an optimization problem. *Environmental Research Letters*, *5*(3). doi: 10.1088/1748-9326/5/3/034009

Bayr, T., Dommenget, D., Martin, T., & Power, S. B. (2014, November). The eastward shift of the Walker Circulation in response to global warming and its relationship to ENSO variability. *Climate Dynamics*, *43*(9), 2747–2763. Retrieved from `https://doi.org/10.1007/s00382-014-2091-y` doi: 10.1007/s00382-014-2091-y

Bednarz, E. M., Butler, A. H., Visioni, D., Zhang, Y., Kravitz, B., & MacMartin, D. G. (2023). Injection strategy – a driver of atmospheric circulation and ozone response to stratospheric aerosol geoengineering. *EGUsphere*, *2023*, 1–32. Retrieved from `https://egusphere.copernicus.org/preprints/2023/egusphere-2023-495/` doi: 10.5194/egusphere-2023-495

Bednarz, E. M., Visioni, D., Richter, J. H., Butler, A. H., & MacMartin, D. G. (2022). Impact of the latitude of stratospheric aerosol injection on the southern annular mode. *Geophysical Research Letters*, *49*(19), e2022GL100353. Retrieved from `https://agupubs.onlinelibrary.wiley.com/doi/abs/10.1029/2022GL100353` (e2022GL100353 2022GL100353) doi: https://doi.org/10.1029/2022GL100353

Boettcher, M., Brent, K., Buck, H. J., Low, S., McLaren, D., & Mengis, N. (2021). Navigating potential hype and opportunity in governing marine carbon removal. *Frontiers in Climate*, *3*. Retrieved from `https://www.frontiersin.org/articles/10.3389/fclim.2021.664456` doi: 10.3389/fclim.2021.664456

Brecha, R. J., Ganti, G., Lamboll, R. D., Nicholls, Z., Hare, B., Lewis, J., ... Gidden, M. J. (2022, August). Institutional decarbonization scenarios evaluated against the Paris Agreement 1.5 °C goal. *Nature Communications*, *13*(1), 4304. Retrieved from `https://doi.org/10.1038/s41467-022-31734-1` doi: 10.1038/s41467-022-31734-1

Cai, W., Santoso, A., Collins, M., Dewitte, B., Karamperidou, C., Kug, J.-S., ... Zhong, W. (2021, September). Changing El Niño–Southern Oscillation in a warming climate. *Nature Reviews Earth & Environment*, *2*(9), 628–

644. Retrieved from https://doi.org/10.1038/s43017-021-00199-z doi: 10.1038/s43017-021-00199-z

Cai, W., Santoso, A., Wang, G., Yeh, S.-W., An, S.-I., Cobb, K. M., ... Wu, L. (2015, September). ENSO and greenhouse warming. *Nature Climate Change*, *5*(9), 849–859. Retrieved from https://doi.org/10.1038/nclimate2743 doi: 10.1038/nclimate2743

Cao, L., Bala, G., Zheng, M., & Caldeira, K. (2015, December). Fast and slow climate responses to CO2 and solar forcing: A linear multivariate regression model characterizing transient climate change. *Journal of Geophysical Research: Atmospheres*, *120*(23), 12,037–12,053. Retrieved 2023-05-24, from https://doi.org/10.1002/2015JD023901 (Publisher: John Wiley & Sons, Ltd) doi: 10.1002/2015JD023901

Crutzen, P. J. (2006). Albedo enhancement by stratospheric sulfur injections: A contribution to resolve a policy dilemma? *Climatic Change*, *77*(3), 211–220. Retrieved from https://doi.org/10.1007/s10584-006-9101-y doi: 10.1007/s10584-006-9101-y

Danabasoglu, G., Lamarque, J.-F., Bacmeister, J., Bailey, D. A., DuVivier, A. K., Edwards, J., ... Strand, W. G. (2020). The Community Earth System Model Version 2 (CESM2). *Journal of Advances in Modeling Earth Systems*, *12*(2), e2019MS001916. doi: https://doi.org/10.1029/2019MS001916

Davis, N. A., Visioni, D., Garcia, R. R., Kinnison, D. E., Marsh, D. R., Mills, M. J., ... Vitt, F. (2022, dec). Climate, variability, and climate sensitivity of "middle atmosphere" chemistry configurations of the community earth system model version 2, whole atmosphere community climate model version 6 (CESM2(WACCM6)). Retrieved from https://doi.org/10.22541\%2Fessoar.167117634.40175082\%2Fv1 doi: 10.22541/essoar.167117634.40175082/v1

DelSole, T., Yan, X., & Tippett, M. K. (2016, September). Inferring Aerosol Cooling from Hydrological Sensitivity. *Journal of Climate*, *29*(17), 6167–6178. Retrieved from https://journals.ametsoc.org/view/journals/clim/29/17/jcli-d-15-0364.1.xml (Place: Boston MA, USA Publisher: American Meteorological Society) doi: 10.1175/JCLI-D-15-0364.1

Fasullo, J. T., & Richter, J. H. (2023). Dependence of strategic solar climate intervention on background scenario and model physics. *Atmospheric Chemistry and Physics*, *23*(1), 163–182. Retrieved from https://acp.copernicus.org/articles/23/163/2023/ doi: 10.5194/acp-23-163-2023

Fasullo, J. T., Simpson, I. R., Kravitz, B., Tilmes, S., Richter, J. H., MacMartin, D. G., & Mills, M. J. (2018). Persistent polar ocean warming in a strategically geoengineered climate. *Nature Geoscience*, *11*(12), 910–914. Retrieved from http://dx.doi.org/10.1038/s41561-018-0249-7 doi: 10.1038/s41561-018-0249-7

Fläschner, D., Mauritsen, T., & Stevens, B. (2016, January). Understanding the Intermodel Spread in Global-Mean Hydrological Sensitivity. *Journal of Climate*, *29*(2), 801–817. Retrieved from https://journals.ametsoc.org/view/journals/clim/29/2/jcli-d-15-0351.1.xml (Place: Boston MA, USA Publisher: American Meteorological Society) doi: 10.1175/JCLI-D-15-0351.1

Gabriel, C. J., & Robock, A. (2015). Stratospheric geoengineering impacts on El Niño/Southern Oscillation. *Atmospheric Chemistry and Physics*, *15*(20), 11949–11966. Retrieved from https://acp.copernicus.org/articles/15/11949/2015/ doi: 10.5194/acp-15-11949-2015

Gao, Y., Gao, X., & Zhang, X. (2017). The 2 °c global temperature target and the evolution of the long-term goal of addressing climate change—from the united nations framework convention on climate change to the paris agreement. *Engineering*, *3*(2), 272-278. Retrieved from https://www.sciencedirect.com/science/article/pii/S2095809917303077 doi: https://doi.org/10.1016/J.ENG.2017.01.022

Govindasamy, B., Caldeira, K., & Duffy, P. (2003). Geoengineering earth's radiation balance to mitigate climate change from a quadrupling of CO2. *Global and Planetary Change*, *37*(1), 157 - 168. Retrieved from http://www.sciencedirect.com/science/article/pii/S0921818102001959 (Evaluation, Intercomparison and Application of Global Climate Models) doi: https://doi.org/10.1016/S0921-8181(02)00195-9

Grothe, P. R., Cobb, K. M., Liguori, G., Di Lorenzo, E., Capotondi, A., Lu, Y., ... Toth, L. T. (2020, April). Enhanced El Niño–Southern Oscillation Variability in Recent Decades. *Geophysical Research Letters*, *47*(7), e2019GL083906. Retrieved 2023-05-24, from https://doi.org/10.1029/2019GL083906 (Publisher: John Wiley & Sons, Ltd) doi: 10.1029/2019GL083906

Guo, A., Moore, J. C., & Ji, D. (2018). Tropical atmospheric circulation response to the G1 sunshade geoengineering radiative forcing experiment. *Atmospheric Chemistry and Physics*, *18*(12), 8689–8706. Retrieved from https://acp.copernicus.org/articles/18/8689/2018/ doi: 10.5194/acp-18-8689-2018

Haszeldine, R. S., Flude, S., Johnson, G., & Scott, V. (2018). Negative emissions technologies and carbon capture and storage to achieve the paris agreement commitments. *Philosophical Transactions of the Royal Society A: Mathematical, Physical and Engineering Sciences*, *376*(2119), 20160447. Retrieved from https://royalsocietypublishing.org/doi/abs/10.1098/rsta.2016.0447 doi: 10.1098/rsta.2016.0447

Held, I. M., & Soden, B. J. (2006, November). Robust Responses of the Hydrological Cycle to Global Warming. *Journal of Climate*, *19*(21), 5686–5699. Retrieved from https://journals.ametsoc.org/view/journals/clim/19/21/jcli3990.1.xml (Place: Boston MA, USA Publisher: American Meteorological Society) doi: 10.1175/JCLI3990.1

Holz, C., Siegel, L. S., Johnston, E., Jones, A. P., & Sterman, J. (2018, June). Ratcheting ambition to limit warming to 1.5 °C–trade-offs between emission reductions and carbon dioxide removal. *Environmental Research Letters*, *13*(6), 064028. Retrieved from https://dx.doi.org/10.1088/1748-9326/aac0c1 (Publisher: IOP Publishing) doi: 10.1088/1748-9326/aac0c1

Irvine, P., Emanuel, K., He, J., Horowitz, L. W., Vecchi, G., & Keith, D. (2019). Halving warming with idealized solar geoengineering moderates key climate hazards. *Nature Climate Change*, *9*(4), 295–299. Retrieved from http://dx.doi.org/10.1038/s41558-019-0398-8 doi: 10.1038/s41558-019-0398-8

Irvine, P. J., & Keith, D. W. (2020, mar). Halving warming with stratospheric aerosol geoengineering moderates policy-relevant climate hazards. *Environmental Research Letters*, *15*(4), 044011. Retrieved from https://dx.doi.org/10.1088/1748-9326/ab76de doi: 10.1088/1748-9326/ab76de

Irvine, P. J., Sriver, R. L., & Keller, K. (2012, February). Tension between reducing sea-level rise and global warming through solar-radiation management. *Nature Climate Change*, *2*(2), 97–100. Retrieved from https://doi.org/10.1038/nclimate1351 doi: 10.1038/nclimate1351

Kang, S. M., Xie, S.-P., Shin, Y., Kim, H., Hwang, Y.-T., Stuecker, M. F., ... Hawcroft, M. (2020). Walker circulation response to extratropical radiative forcing. *Science Advances*, *6*(47), eabd3021. Retrieved from https://www.science.org/doi/abs/10.1126/sciadv.abd3021 doi: 10.1126/sciadv.abd3021

Kravitz, B., Lamarque, J.-F., Tribbia, J. J., Tilmes, S., Vitt, F., Richter, J. H., ... Mills, M. J. (2017). First Simulations of Designing Stratospheric Sulfate Aerosol Geoengineering to Meet Multiple Simultaneous Climate Objectives. *Journal of Geophysical Research: Atmospheres*, *122*(23), 12,616–12,634. doi: 10.1002/2017jd026874

Kravitz, B., MacMartin, D. G., Tilmes, S., Richter, J. H., Mills, M. J., Cheng, W.,

… Vitt, F. (2019). Comparing surface and stratospheric impacts of geoengineering with different SO2 injection strategies. *Journal of Geophysical Research: Atmospheres*, *124*(14), 7900-7918. Retrieved from https://agupubs.onlinelibrary.wiley.com/doi/abs/10.1029/2019JD030329 doi: 10.1029/2019JD030329

Kravitz, B., Robock, A., Tilmes, S., Boucher, O., English, J. M., Irvine, P. J., … Watanabe, S. (2015). The geoengineering model intercomparison project phase 6 (GeoMIP6): simulation design and preliminary results. *Geoscientific Model Development*, *8*(10), 3379–3392. Retrieved from https://gmd.copernicus.org/articles/8/3379/2015/ doi: 10.5194/gmd-8-3379-2015

Kriegler, E., Luderer, G., Bauer, N., Baumstark, L., Fujimori, S., Popp, A., … van Vuuren, D. P. (2018). Pathways limiting warming to 1.5°c: a tale of turning around in no time? *Philosophical Transactions of the Royal Society A: Mathematical, Physical and Engineering Sciences*, *376*(2119), 20160457. Retrieved from https://royalsocietypublishing.org/doi/abs/10.1098/rsta.2016.0457 doi: 10.1098/rsta.2016.0457

Kvalevåg, M. M., Samset, B. H., & Myhre, G. (2013, April). Hydrological sensitivity to greenhouse gases and aerosols in a global climate model. *Geophysical Research Letters*, *40*(7), 1432–1438. Retrieved 2023-05-24, from https://doi.org/10.1002/grl.50318 (Publisher: John Wiley & Sons, Ltd) doi: 10.1002/grl.50318

Laakso, A., Niemeier, U., Visioni, D., Tilmes, S., & Kokkola, H. (2022). Dependency of the impacts of geoengineering on the stratospheric sulfur injection strategy – part 1: Intercomparison of modal and sectional aerosol modules. *Atmospheric Chemistry and Physics*, *22*(1), 93–118.

Lenton, T. M., Held, H., Kriegler, E., Hall, J. W., Lucht, W., Rahmstorf, S., & Schellnhuber, H. J. (2008). Tipping elements in the earth's climate system. *Proceedings of the National Academy of Sciences*, *105*(6), 1786-1793. Retrieved from https://www.pnas.org/doi/abs/10.1073/pnas.0705414105 doi: 10.1073/pnas.0705414105

Liu, X., Ma, P.-L., Wang, H., Tilmes, S., Singh, B., Easter, R. C., … Rasch, P. J. (2016). Description and evaluation of a new four-mode version of the Modal Aerosol Module (MAM4) within version 5.3 of the Community Atmosphere Model. *Geoscientific Model Development*, *9*(2), 505–522. doi: 10.5194/gmd-9-505-2016

MacMartin, D. G., Kravitz, B., Mills, M. J., Tribbia, J. J., Tilmes, S., Richter, J. H., … Lamarque, J.-F. (2017). The Climate Response to Stratospheric Aerosol Geoengineering Can Be Tailored Using Multiple Injection Locations. *Journal of Geophysical Research: Atmospheres*, *122*(23), 12,574–12,590. doi: 10.1002/2017jd026868

MacMartin, D. G., Ricke, K. L., & Keith, D. W. (2018). Solar geoengineering as part of an overall strategy for meeting the 1.5°c paris target. *Philosophical Transactions of the Royal Society A: Mathematical, Physical and Engineering Sciences*, *376*(2119), 20160454. Retrieved from https://royalsocietypublishing.org/doi/abs/10.1098/rsta.2016.0454 doi: 10.1098/rsta.2016.0454

MacMartin, D. G., Visioni, D., Kravitz, B., Richter, J., Felgenhauer, T., Lee, W. R., … Sugiyama, M. (2022). Scenarios for modeling solar radiation modification. *Proceedings of the National Academy of Sciences*, *119*(33), e2202230119. Retrieved from https://www.pnas.org/doi/abs/10.1073/pnas.2202230119 doi: 10.1073/pnas.2202230119

Malik, A., Nowack, P. J., Haigh, J. D., Cao, L., Atique, L., & Plancherel, Y. (2020). Tropical Pacific climate variability under solar geoengineering: impacts on ENSO extremes. *Atmospheric Chemistry and Physics*, *20*(23), 15461–15485.

Retrieved from https://acp.copernicus.org/articles/20/15461/2020/ doi: 10.5194/acp-20-15461-2020

Masson-Delmotte, V., et al. (Eds.). (2018). *Global Warming of 1.5°C: An IPCC Special Report on the impacts of global warming of 1.5°C above pre-industrial levels and related global greenhouse gas emission pathways, in the context of strengthening the global response to the threat of climate change, sustainable development, and efforts to eradicate poverty.* Geneva, Switzerland: World Meteorological Organization. Retrieved from https://www.ipcc.ch/sr15/

Meinshausen, M., Nicholls, Z. R. J., Lewis, J., Gidden, M. J., Vogel, E., Freund, M., ... Wang, R. H. J. (2020). The shared socio-economic pathway (ssp) greenhouse gas concentrations and their extensions to 2500. *Geoscientific Model Development*, *13*(8), 3571–3605. Retrieved from https://gmd.copernicus.org/articles/13/3571/2020/ doi: 10.5194/gmd-13-3571-2020

Niemeier, U., Schmidt, H., Alterskjær, K., & Kristjánsson, J. E. (2013). Solar irradiance reduction via climate engineering: Impact of different techniques on the energy balance and the hydrological cycle. *Journal of Geophysical Research: Atmospheres*, *118*(21), 11,905-11,917. Retrieved from https://agupubs.onlinelibrary.wiley.com/doi/abs/10.1002/2013JD020445 doi: 10.1002/2013JD020445

Niemeier, U., & Timmreck, C. (2015). What is the limit of climate engineering by stratospheric injection of SO2? *Atmospheric Chemistry and Physics*, *15*(16), 9129–9141. Retrieved from https://www.atmos-chem-phys.net/15/9129/2015/ doi: 10.5194/acp-15-9129-2015

Nowack, P. J., Luke Abraham, N., Maycock, A. C., Braesicke, P., Gregory, J. M., Joshi, M. M., ... Pyle, J. A. (2015, January). A large ozone-circulation feedback and its implications for global warming assessments. *Nature Climate Change*, *5*(1), 41–45. Retrieved from https://doi.org/10.1038/nclimate2451 doi: 10.1038/nclimate2451

Pendergrass, A. G., & Hartmann, D. L. (2014, January). The Atmospheric Energy Constraint on Global-Mean Precipitation Change. *Journal of Climate*, *27*(2), 757–768. Retrieved from https://journals.ametsoc.org/view/journals/clim/27/2/jcli-d-13-00163.1.xml (Place: Boston MA, USA Publisher: American Meteorological Society) doi: 10.1175/JCLI-D-13-00163.1

Rajamani, L., & Werksman, J. (2018). The legal character and operational relevance of the paris agreement's temperature goal. *Philosophical Transactions of the Royal Society A: Mathematical, Physical and Engineering Sciences*, *376*(2119), 20160458. Retrieved from https://royalsocietypublishing.org/doi/abs/10.1098/rsta.2016.0458 doi: 10.1098/rsta.2016.0458

Reynolds, J. L. (2022). Communication of solar geoengineering science: Forms, examples, and explanation of skewing. *The Anthropocene Review*, *0*(0), 20530196221095569. Retrieved from https://doi.org/10.1177/20530196221095569 doi: 10.1177/20530196221095569

Ricke, K., Wan, J. S., Saenger, M., & Lutsko, N. J. (2023). Hydrological consequences of solar geoengineering. *Annual Review of Earth and Planetary Sciences*, *51*(1), null. Retrieved from https://doi.org/10.1146/annurev-earth-031920-083456 doi: 10.1146/annurev-earth-031920-083456

Robock, A., Oman, L., & Stenchikov, G. L. (2008). Regional climate responses to geoengineering with tropical and arctic so2 injections. *Journal of Geophysical Research: Atmospheres*, *113*(D16). Retrieved from https://agupubs.onlinelibrary.wiley.com/doi/abs/10.1029/2008JD010050 doi: https://doi.org/10.1029/2008JD010050

Samset, B. H., Myhre, G., Forster, P. M., Hodnebrog, Ø., Andrews, T., Boucher, O., ... Voulgarakis, A. (2018, January). Weak hydrological sensitivity to temperature change over land, independent of climate forcing. *npj Climate and Atmospheric Science*, *1*(1), 20173. Retrieved from https://doi.org/

10.1038/s41612-017-0005-5 doi: 10.1038/s41612-017-0005-5

Simpson, I., Tilmes, S., Richter, J., Kravitz, B., MacMartin, D., Mills, M., ... Pendergrass, A. (2019). The regional hydroclimate response to stratospheric sulfate geoengineering and the role of stratospheric heating. *Journal of Geophysical Research: Atmospheres*, 2019JD031093. Retrieved from https://onlinelibrary.wiley.com/doi/abs/10.1029/2019JD031093 doi: 10.1029/2019JD031093

Tilmes, S., Fasullo, J., Lamarque, J.-F., Marsh, D. R., Mills, M., Alterskjær, K., ... Watanabe, S. (2013). The hydrological impact of geoengineering in the geoengineering model intercomparison project (GeoMIP). *Journal of Geophysical Research: Atmospheres*, *118*(19), 11,036-11,058. Retrieved from https://agupubs.onlinelibrary.wiley.com/doi/abs/10.1002/jgrd.50868 doi: 10.1002/jgrd.50868

Timmermann, A., An, S.-I., Kug, J.-S., Jin, F.-F., Cai, W., Capotondi, A., ... Zhang, X. (2018, July). El Niño–Southern Oscillation complexity. *Nature*, *559*(7715), 535–545. Retrieved from https://doi.org/10.1038/s41586-018-0252-6 doi: 10.1038/s41586-018-0252-6

Vecchi, G. A., Soden, B. J., Wittenberg, A. T., Held, I. M., Leetmaa, A., & Harrison, M. J. (2006, May). Weakening of tropical Pacific atmospheric circulation due to anthropogenic forcing. *Nature*, *441*(7089), 73–76. Retrieved from https://doi.org/10.1038/nature04744 doi: 10.1038/nature04744

Visioni, D. (2022). *Data from: Scenarios for modeling solar radiation modification.* doi: https://doi.org/10.7298/xr82-sv86

Visioni, D., Bednarz, E. M., Lee, W. R., Kravitz, B., Jones, A., Haywood, J. M., & MacMartin, D. G. (2023). Climate response to off-equatorial stratospheric sulfur injections in three earth system models – part 1: Experimental protocols and surface changes. *Atmospheric Chemistry and Physics*, *23*(1), 663–685. Retrieved from https://acp.copernicus.org/articles/23/663/2023/ doi: 10.5194/acp-23-663-2023

Visioni, D., MacMartin, D. G., & Kravitz, B. (2021). Is turning down the sun a good proxy for stratospheric sulfate geoengineering? *Journal of Geophysical Research: Atmospheres*, *126*(5), e2020JD033952. Retrieved from https://agupubs.onlinelibrary.wiley.com/doi/abs/10.1029/2020JD033952 (e2020JD033952 2020JD033952) doi: https://doi.org/10.1029/2020JD033952

Visioni, D., MacMartin, D. G., Kravitz, B., Boucher, O., Jones, A., Lurton, T., ... Tilmes, S. (2021). Identifying the sources of uncertainty in climate model simulations of solar radiation modification with the g6sulfur and g6solar geoengineering model intercomparison project (geomip) simulations. *Atmospheric Chemistry and Physics*, *21*(13), 10039–10063. Retrieved from https://acp.copernicus.org/articles/21/10039/2021/ doi: 10.5194/acp-21-10039-2021

Visioni, D., MacMartin, D. G., Kravitz, B., Lee, W., Simpson, I. R., & Richter, J. H. (2020). Reduced poleward transport due to stratospheric heating under stratospheric aerosols geoengineering. *Geophysical Research Letters*, *n/a*(n/a), e2020GL089470. Retrieved from https://agupubs.onlinelibrary.wiley.com/doi/abs/10.1029/2020GL089470 (e2020GL089470 2020GL089470) doi: 10.1029/2020GL089470

Visioni, D., MacMartin, D. G., Kravitz, B., Richter, J. H., Tilmes, S., & Mills, M. J. (2020). Seasonally modulated stratospheric aerosol geoengineering alters the climate outcomes. *Geophysical Research Letters*, *n/a*(n/a), e2020GL088337. Retrieved from https://agupubs.onlinelibrary.wiley.com/doi/abs/10.1029/2020GL088337 (e2020GL088337 2020GL088337) doi: 10.1029/2020GL088337

Warszawski, L., Kriegler, E., Lenton, T. M., Gaffney, O., Jacob, D., Klingenfeld, D., ... Rockström, J. (2021, May). All options, not silver bullets, needed to limit global warming to 1.5 °C: a scenario appraisal. *Environmental Research Letters*, *16*(6), 064037. Retrieved from https://dx.doi.org/10.1088/1748-9326/abfeec (Publisher: IOP Publishing) doi: 10.1088/1748-9326/abfeec

Zhang, Y., MacMartin, D. G., Visioni, D., Bednarz, E., & Kravitz, B. (2023). Introducing a Comprehensive Set of Stratospheric Aerosol Injection Strategies. *EGUsphere*, *2023*, 1–32. Retrieved from https://egusphere.copernicus.org/preprints/2023/egusphere-2023-117/ doi: 10.5194/egusphere-2023-117

Supplementary material to "The choice of baseline period influences the assessments of the outcomes of Stratospheric Aerosol Injection"

	2020-2039 (1.5)	2008-2027 (1.0)	1993-2012 (0.5)
dT1/dT0	0.25	0.28	0.33
dT2/dT0	0.39	0.36	0.32

Table S1 Values for the ratios dT1/dT0 and dT2/dT0, which explain the distribution on SO2 between the injection locations as explained in Section 3.1.

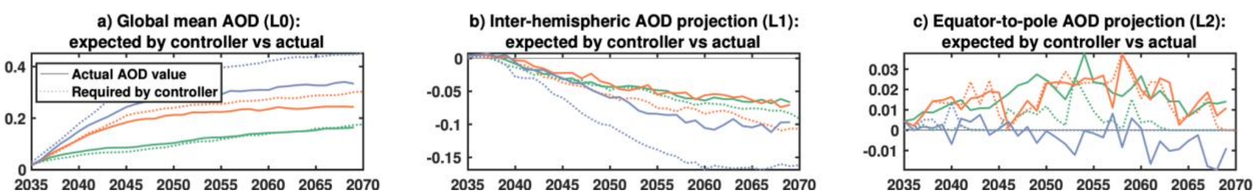

Fig S1 As in Fig.1, panels c-e) Values of L0 (global mean sAOD), L1 (inter-hemispheric sAOD projection) and L2 (equator-to-pole sAOD projection), but with added lines for the values as required by the feedback controller (dashed lines) as opposed to the ones actually simulated by the model.

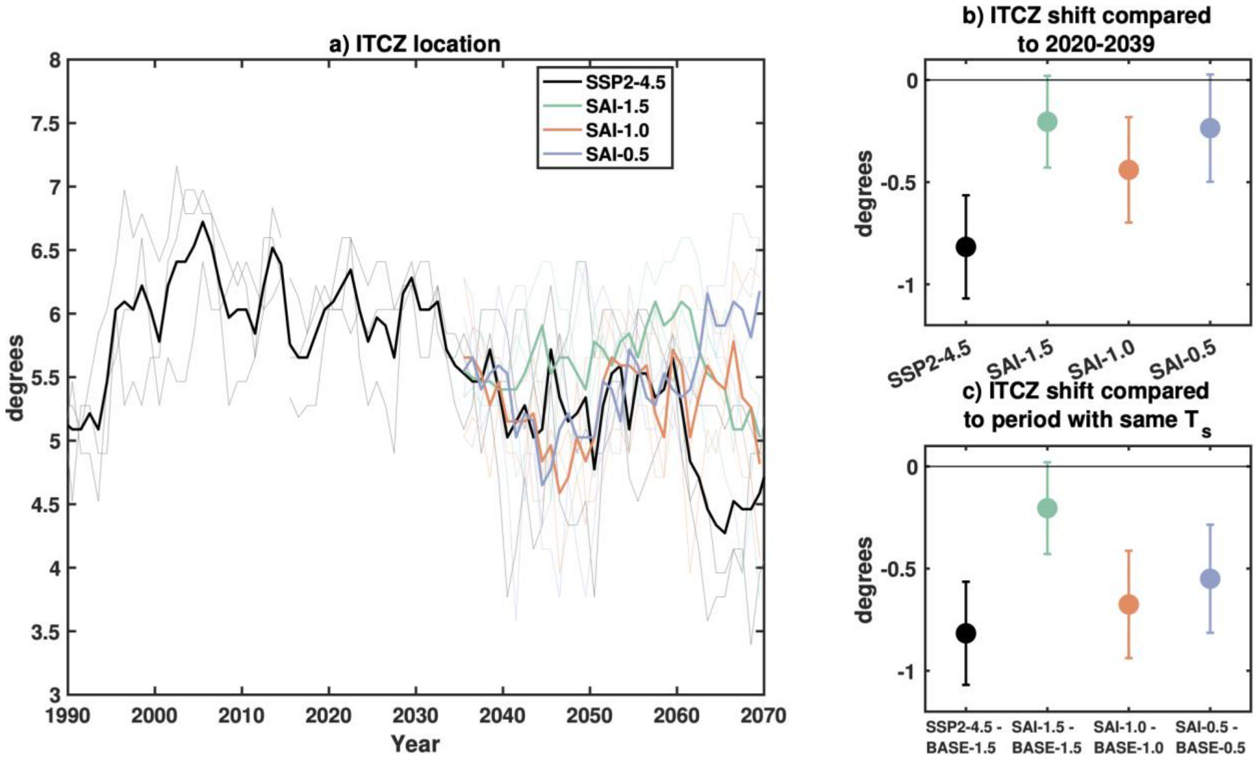

Figure S2. a) Annual mean ITCZ location for all experiments, with a moving average of 5 years applied for smoothing. b) Annual mean changes in the location of ITCZ (degrees) in 2050-2069 compared to the values in the period 2020-2039, approximated as the latitude around the equator where the meridional mass streamfunction at 500 hPa changes sign.c) Annual mean changes in the location of ITCZ (degrees) in 2050-2069 for the three SAI simulations compared to their respective temporal period with the same global mean surface temperature Error bars denote ±1 standard errors in the difference in means.

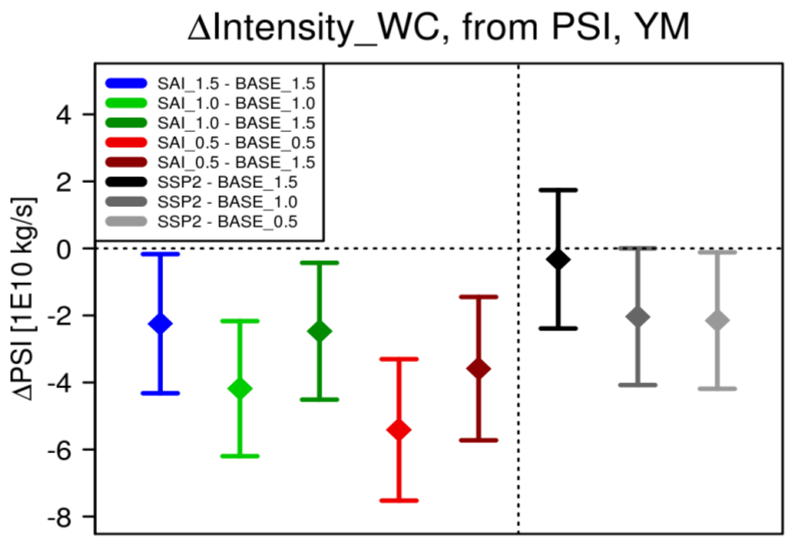

Figure S3. As in Figure 5 (left panel) but for the changes in Walker Circulation calculated as difference between zonal mass streamfunction at 400 hPa, averaged between 10S-10N, between Western Pacific (180E-240E) and Indian Ocean (60-120E).

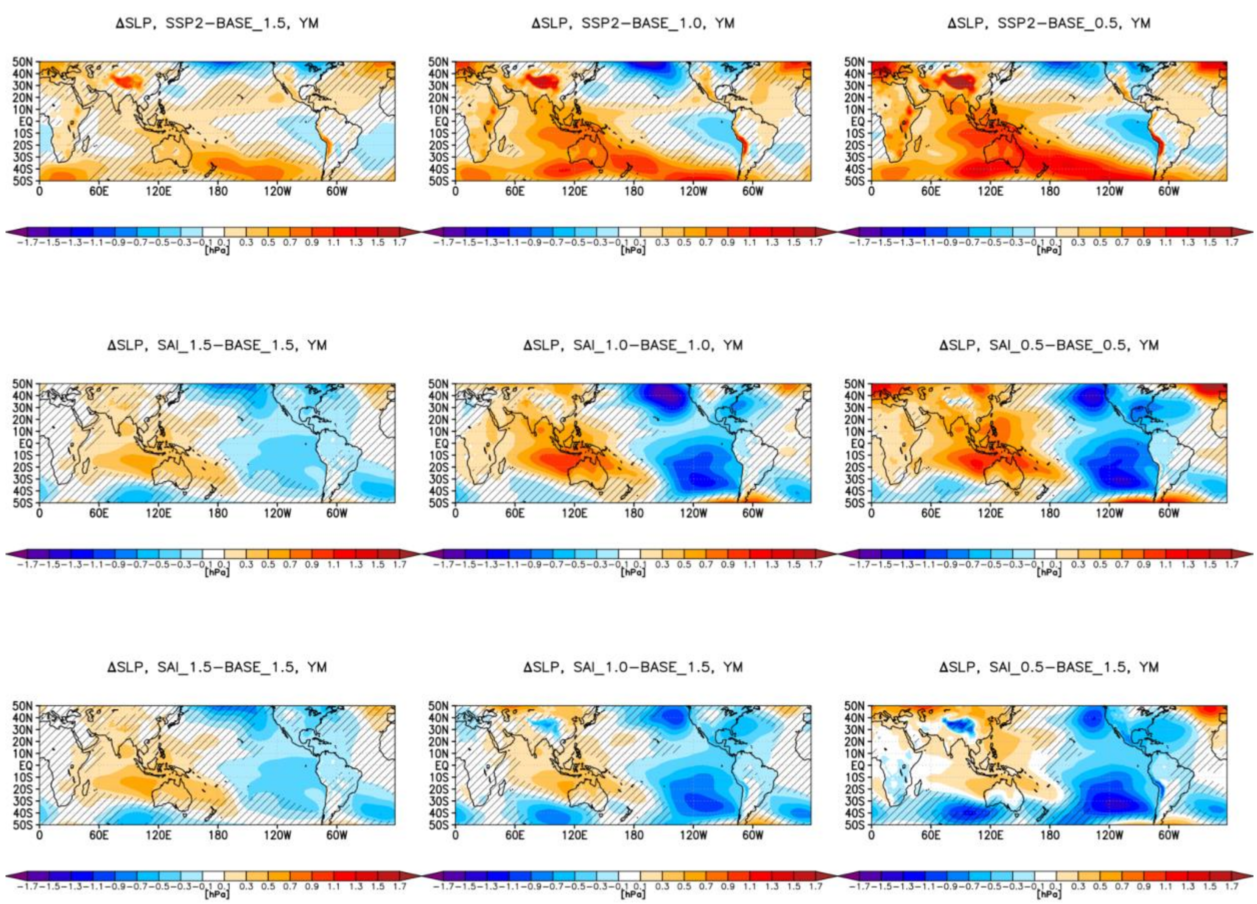

Figure S4. Annual mean changes in SLP (hPa).

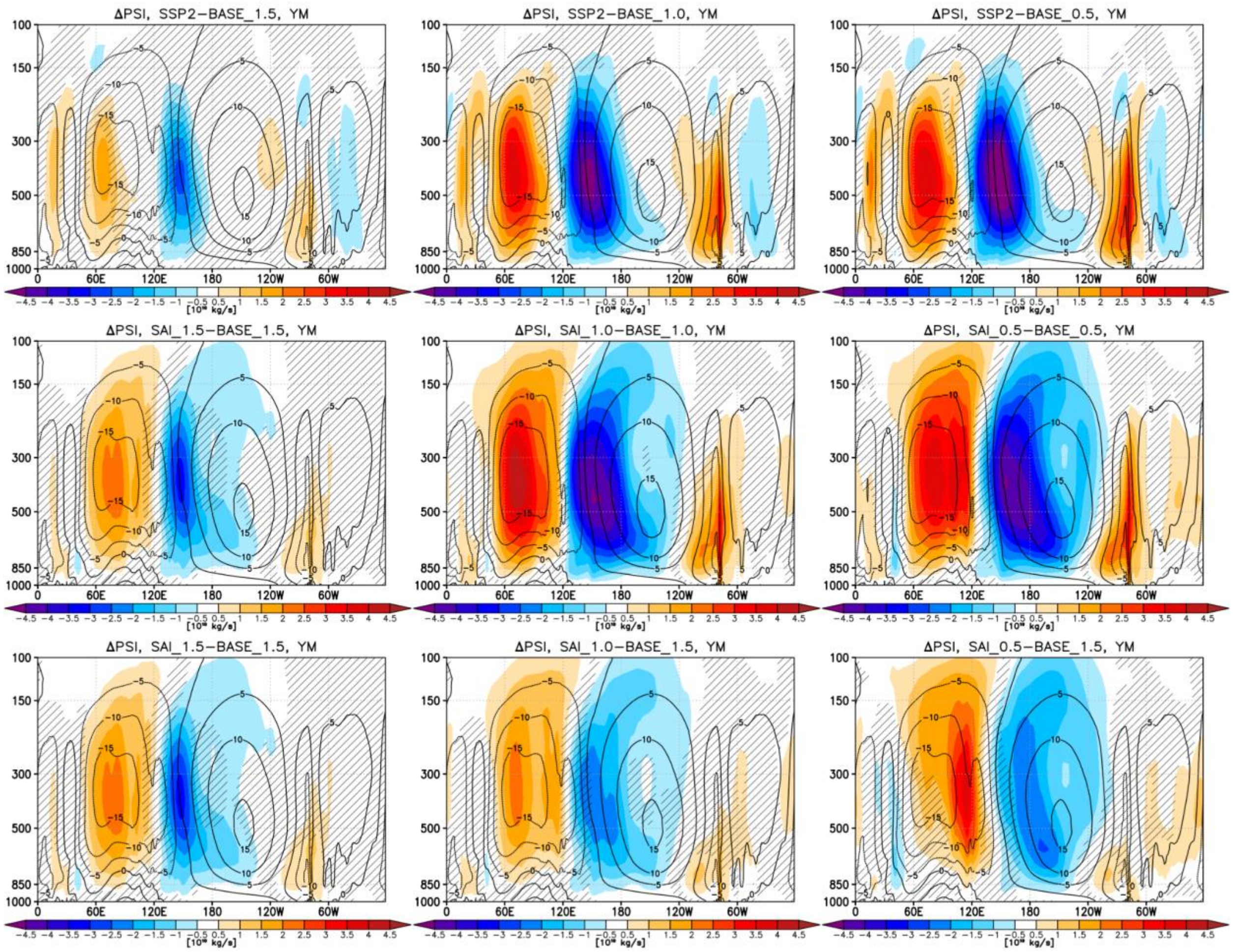

Figure S5. Annual mean changes in zonal mass stream function (10^{10} kg/s)**.**